Bioorganic Chemistry 180 (2026) 110166

Contents lists available at ScienceDirect

Bioorganic Chemistry

journal homepage: www.elsevier.com/locate/bioorg

Design, synthesis, and pharmacological evaluation of thiazolo[5,4-*d*]pyrimidines hybridized with lipoic acid or catechol. Novel A_{2A} adenosine receptor antagonists in neuroinflammatory diseases

Sara Calenda [a,1], Katarina Mihajlovic [b,1], Flavia Varano [a], Daniela Catarzi [a], Costanza Ceni [a], Elisa Marinari [a], Giulia Vagnoni [a], Marta Menicatti [a], Gian Luca Bartolucci [a], Diego Dal Ben [c], Rosaria Volpini [c], Katia Varani [d], Chiara Contri [d], Fabrizio Vincenzi [d], Ana Martinez [e,f], Loreto Martinez Gonzales [e,f], Milorad Dragic [b,g], Miloš Mojović [h], Đura Nakarada [h], Ivana Stevanovic [i], Nadežda Nedeljkovic [b,2], Vittoria Colotta [a,*,2]

[a] *Department of NEUROFARBA, Pharmaceutical and Nutraceutical Section, University of Florence, Via Ugo Schiff, 6, 50019 Sesto Fiorentino, FI, Italy.*
[b] *Center for Translational Neurosciences, Department of General Physiology and Biophysics, Faculty of Biology, University of Belgrade, Studentski trg 3, 11158 Belgrade, Serbia*
[c] *Medicinal Chemistry Unit, School of Pharmacy, University of Camerino, Via Madonna delle Carceri, 9, 62032 Camerino, Italy*
[d] *Department of Translational Medicine, University of Ferrara, via Luigi Borsari, 46, 44121 Ferrara, Italy*
[e] *Centro de Investigaciones Biológicas, CSIC-c/ Ramiro de Maetzu 9, 28040 Madrid, Spain*
[f] *Centro de Investigación Biomédica en Red de Enfermedades Neurodegenerativas (CIBERNED), Instituto Carlos III, 28031 Madrid, Spain*
[g] *Vinca Institute for Nuclear Sciences - National Institute of the Republic of Serbia, University of Belgrade, Serbia*
[h] *Center for Physical Chemistry of Biological Systems, BioScope Labs, Faculty of Physical Chemistry, University of Belgrade, 11158 Belgrade, Serbia*
[i] *Medical Faculty of Military Medical Academy, University of Defence, Belgrade, Serbia*

ARTICLE INFO

Keywords:
A_{2A} adenosine receptor antagonists
Antioxidants
Multitarget approach
Oxidative stress
Inflammation

ABSTRACT

Oxidative stress and inflammation are closely interconnected processes involved in the pathogenesis of neurodegenerative diseases. Adenosine, acting through the A_{2A} receptor subtype, plays a crucial role in inflammatory processes, making A_{2A} adenosine receptor (AR) antagonists promising therapeutic candidates. In this study, we designed and synthesized three thiazolo[5,4-*d*]pyrimidine derivatives incorporating antioxidant moieties, namely catechol (compound **1**) and lipoic acid (compounds **2** and **3**), to obtain ligands combining A_{2A} AR antagonism with antioxidant activity.

All compounds displayed nanomolar affinity and antagonist activity at the A_{2A} AR, while compound **1** also exhibited activity at the A_{2B} AR. In cell-free assays (DPPH), compound **1** showed pronounced radical-scavenging activity. In LPS-stimulated BV2 microglial cells, the derivatives significantly reduced nitric oxide production and

Abbreviations: ABMECA, N^6-(4-aminobenzyl)-*N*-methylcarboxamidoadenosine; ADME, Absorption, distribution, metabolism, excretion; AR, Adenosine receptor; BBB, Blood brain barrier; CAT, Catalase; CC, Carbon-centered; COX-2, Cyclooxygenase 2; CV, Crystal violet; DEPMPO, 5-(Diethoxyphosphoryl)-5-methyl-1-pyrroline-N-oxide; DHLA, Dihydrolipoic acid; DPCPX, 8-cyclopentyl-1,3-dipropylxanthine; DPPH, 2,2-Diphenyl-1-picrylhydrazyl; EAE, Experimental autoimmune encephalomyelitis; EDA, Edaravone; EDCI, 1-(3-(dimethylamino)-propyl))-3-ethylcarbodiimide; EL, Extracellular loop; ELISA, Enzyme-linked immunosorbent assay; EPR, Electron paramagnetic resonance; ESI, Electrospray ionization source; FWHM, Full width at half maximum; GSH, Glutathione; HOBt, 1-hydroxybenzotriazole; HRMS, High-resolution mass spectrometry; IL-6, Interleukin 6; IL-10, Interleukin 10; iNOS/NOS2, Inducible nitric oxide synthase; IS, Internal standard; LA, Lipoic acid; LPS, Lipopolysaccharide; MAPK, Mitogen-activated protein kinase; MDA, Malondialdheyde; MOE, Molecular operating environment; MS, Multiple sclerosis; MTT, 3-(4,5-dimethyl-2-thiazolyl) 2,5-diphenyl-2-H-tetrazolium bromide; NBS, N-bromosuccinimide; NBT, Nitroblue-tetrazolium; NECA, 5-(N-ethyl-carboxamido)adenosine; NO, Nitric oxide; OD, Optical density; p, Phosphorylated; PBL, Polar brain lipid; PBS, Phosphate saline buffer; Pe, Permeability; PLO, Poly-L-ornithine; PMA, Phorbol 12-myristate 13-acetate; RDB, Double bond/ring equivalents; RNS, Reactive nitrogen species; RSA, Radical scavenging ability; Rt, Room temperature; SD, Standard deviation; SE, Standard error; SEM, Standard error of the mean; TBA, Thiobarbituric acid; TBST, Tris-buffer saline/tween 20; TNF-α, Tumor necrosis factor alpha; tSOD, Total superoxide dismutase.

* Corresponding author.
E-mail address: vittoria.colotta@unifi.it (V. Colotta).
[1] Co-first authors.
[2] Co-last authors.

https://doi.org/10.1016/j.bioorg.2026.110166
Received 15 May 2026; Received in revised form 16 June 2026; Accepted 23 June 2026
Available online 25 June 2026

improved microglial morphology. Furthermore, the compounds enhanced the release of anti-inflammatory cytokines. Notably, compound **1** markedly decreased ERK phosphorylation levels, indicating modulation of intracellular inflammatory signaling pathways.

Overall, these results highlight the potential of thiazolo[5,4-*d*]pyrimidine-based hybrids as anti-inflammatory A_{2A} AR antagonists, supporting further investigation of this series for the development of new strategies for the treatment of neuroinflammatory diseases.

1. Introduction

At present, inflammatory processes and neurodegeneration have been recognized as closely interconnected. Several studies have shown that inflammation plays a key role in the onset and progression of neurodegenerative diseases, such as multiple sclerosis (MS), through the activation of immune cells, such as T and B lymphocytes and microglia, as well as the release of inflammatory mediators, including reactive oxygen and nitrogen species, pro-inflammatory cytokines, and antibodies [1]. The relationship between inflammation and disease status in MS has been analyzed by examining demyelinating lesions. Evidence indicates that the density of T- and B-cells infiltrates correlates with the activity of demyelinating lesions observed in the early stages of the pathology, thus suggesting that the therapeutic intervention targeting inflammatory processes may be most effective at the onset of the disease [2]. Due to the link between neuroinflammation and neurodegeneration, immune-directed therapies have been developed to treat MS, targeting both peripheral immune cells and inflammatory pathways in the central nervous system (CNS), including glia-driven signaling processes [3].

Adenosine is a key endogenous modulator that regulates multiple physiological effects (e.g., inflammation, locomotion, sleep, behaviour, and nociception) [4,5] through the activation of its four G-protein-coupled receptors (ARs) named A_1, A_{2A}, A_{2B}, and A_3. ARs modulate the production of cyclic adenosine monophosphate (cAMP). Specifically, while A_1 and A_3 AR subtypes are negatively coupled with adenylyl cyclase, thus determining an inhibitory effect on cAMP production, A_{2A} and A_{2B} ARs induce an increase in cAMP production by stimulating the activity of adenylyl cyclase [6,7]. In addition to regulating intracellular cAMP levels, ARs can engage several downstream signaling pathways involved in neuroinflammation. Among these, the mitogen-activated protein kinase (MAPK) cascade, including extracellular signal-regulated kinases 1 and 2 (ERK1/2), plays a central role in the regulation of inflammatory gene expression, cytokine production, and microglial activation. A_{2A} and A_{2B} ARs have been reported to modulate ERK signaling in both neural and immune cells, suggesting that regulation of the MAPK/ERK pathway may contribute to the anti-inflammatory effects mediated by these ARs [8]. Among the ARs, A_1 and A_{2A} are the most abundant subtypes in the CNS [9], and have therefore received considerable attention in research on neurodegenerative disorders. In particular, the A_{2A} subtype is the most extensively investigated in the context of neuroinflammation and has emerged as an attractive therapeutic target. However, growing evidence indicates that the A_1 AR is also implicated in the modulation of microglial activity and inflammatory signaling, although its role remains controversial, highly context-dependent, and incompletely understood [8,10,11]. The A_{2B} AR subtype is expressed at lower levels in the brain than the A_1 and A_{2A} ARs under physiological conditions, but its contribution becomes increasingly relevant under pathological conditions, as it is markedly upregulated in glial and vascular endothelial cells in response to hypoxia, ischemia, and neuroinflammation [12]. Two models of neuroinflammation highlighted the anti-inflammatory effect of the potent A_{2A} AR antagonist SCH-58261 in reducing excitotoxicity in primary microglial cells derived from rats [13]. Similar to A_{2A} AR antagonists, the use of A_{2B} AR antagonists (CVT6883 and MRS1754) in experimental autoimmune encephalomyelitis (EAE), an animal model of MS, has led to an improvement in clinical symptoms, accompanied by a reduction in the pro-inflammatory cytokine interleukin 6 (IL-6) [14].

Oxidative stress is a key risk factor for neurodegenerative diseases. It arises from an imbalance between the production and the elimination of reactive species and can trigger inflammatory processes [15]. In this scenario, the use of antioxidants has gained recognition as a treatment for neurodegenerative disorders, as they may inhibit early pro-inflammatory events. Polyphenols are a class of antioxidants, well known for their radical scavenging activity against reactive oxygen species (ROS). In addition, they can modulate the activity of enzymes involved in oxidative pathways, such as cyclooxygenase, lipoxygenase, and nitric oxide synthases, as well as regulate some inflammatory pathways (such as the NLRP3 inflammasome) [16]. Among polyphenols, simple catechol derivatives proved to be effective in reducing the production of nitric oxide (NO), a key marker of inflammation, and the proinflammatory cytokine tumor necrosis factor (TNF)-α in lipopolysaccharide (LPS)-stimulated BV2 microglial cells [17]. Alpha-lipoic acid (**LA**) is another potent antioxidant, owing to its ability to act both as a radical scavenger in its reduced form, dihydrolipoic acid (DHLA), and as an anti-inflammatory agent [18]. Since many neurological disorders, such as MS, are characterized by severe oxidative stress and inflammation [15], **LA** has been extensively investigated as a therapeutic option. Treatment with **LA** in EAE reduced immune cell infiltration in the CNS, suggesting that **LA** could improve the condition of patients with MS [19].

Considering this evidence and the multifactorial nature of neurodegenerative diseases, part of our recent research has focused on the design and synthesis of hybrid compounds capable of both antagonizing the A_{2A} AR and exerting antioxidant effects [20,21]. In a recent study, we reported the synthesis of the thiazolo[5,4-*d*]pyrimidine derivative **P686**, obtained through the hybridization of a highly potent A_{2A} AR antagonist (Fig. 1, derivative **A**) with the antioxidant edaravone (EDA). This site of hybridization was suggested by structure-affinity relationship studies within this series, which indicate that the introduction of bulky groups

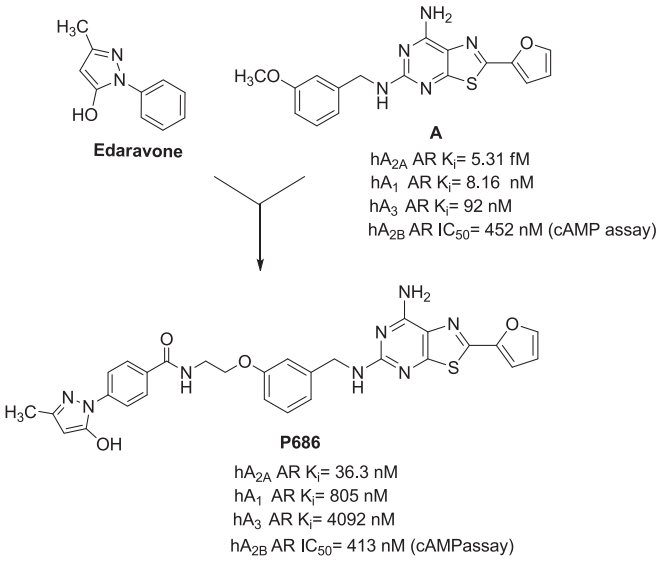

Fig. 1. Structures of the previously reported thiazolo[5,4-*d*]pyrimidine derivative **A** and the EDA–hybrid derivative **P686**.

at position 5 of the scaffold does not compromise A_{2A} AR affinity and may even enhance A_{2A} AR selectivity. Accordingly, computational studies showed that the most favorable binding pose features the 2-furyl ring deeply oriented within the receptor cavity, while the bulky 5-substituent points toward the extracellular environment, thus not hindering receptor-ligand interactions [22]. Derivative **P686** exhibited good hA_{2A} AR affinity and selectivity, promoted in vitro oligodendrocyte differentiation and enhanced myelination processes [23].

In the present study, the 5-(3-methoxybenzylamino)-substituted thiazolo[5,4-*d*]pyrimidine derivative **A** [24] was hybridized with the antioxidants catechol and **LA** yielding compounds **1** and **2** (Fig. 2). In addition, the hybrid **3**, regioisomer of derivative **2**, was also synthesized. Compounds **2** and **3** bear a LA moiety attached to the 5-benzylamino group through the same linker previously employed in derivative **P686**.

2. Results and discussion

2.1. Chemistry

Derivatives **1–3** were synthesized as described in Schemes 1–2. The catechol derivative **1** was obtained as depicted in Scheme 1. The commercial 3,4-dimethoxybenzylamine **6** was reacted, under microwave (MW) irradiation, with the 7-amino-5-chlorothiazolo[5,4-*d*]pyrimidine [24] to give the dimethoxy derivative **8,** which was hydrolyzed with a BBr_3 solution in CH_2Cl_2, to give the catechol derivative **1**.

The thiazolopyrimidines **2** and **3** were synthesized as shown in Scheme 2, by reacting, respectively, the 3-(2-aminoethoxy)benzyl derivative **4** and/or its regioisomer **5** with (*R,S*) **LA**, in the presence of 1-(3-(dimethylamino)-propyl))-3-ethylcarbodiimide (EDCI) hydrochloride, 1-hydroxybenzotriazole (HOBt), and Et_3N in anhydrous DMF. Derivative **4** was prepared as previously described [23], while **5** was newly synthesized starting from N-Boc benzylamine derivative **9** [25] which was deprotected to give derivative **10**. Reaction of **10** with the thiazolopyrimidine **7**, carried out under microwave irradiation and in the presence of Et_3N, yielded the hydroxy derivative **11,** which was brominated to give **12**. Reaction of the latter with a saturated ethanol solution of ammonia yielded the amine derivative **5**.

2.2. Structure-affinity relationships

The new hybrid derivatives **1–3** were evaluated for their binding affinity at hA_1, hA_{2A} and hA_3 ARs, and for their functional antagonistic activity at hA_{2A} and hA_{2B} ARs. The thiazolopyrimidines **4** and **5**, which are synthetic intermediates, were also tested, as they were expected to exhibit AR affinity. The results are summarized in Table 1.

As expected, all derivatives **1–5** exhibited high hA_{2A} AR affinity and potency, and, generally, also good to high hA_{2A} AR selectivity vs the other AR subtypes. The thiazolopyrimidine **1**, featuring the catechol ring, showed the highest hA_{2A} AR affinity (K_i = 10.1 nM), among the herein reported derivatives, and different selectivity versus A_1 AR (27-fold) and A_3 AR (13-fold). Compound **1** proved to be a potent hA_{2A} AR antagonist in the cAMP assay (IC_{50} = 22.7 nM). It was also able to bind the hA_{2B} AR subtype and to reduce with a good potency 5-(N-ethyl-carboxamido)adenosine (NECA)-induced cAMP accumulation in hA_{2B}-CHO cells (IC_{50} = 84.5 nM). This behaviour makes **1** a dual hA_{2A}/hA_{2B} AR antagonist. Both the LA hybridized-thiazolopyrimidines **2** and **3** showed high affinity for the hA_{2A} AR, with **2** being more active (K_i = 16.4 nM) than **3** (K_i = 39.8 nM). Both derivatives **2** and **3** exhibited high hA_{2A} AR selectivity versus hA_1 and hA_3 ARs, and in functional tests they proved to be hA_{2A} AR antagonists, with compound **2** (IC_{50} = 34.1 nM) being about 3-fold more potent than **3** (IC_{50} = 101 nM). Compounds **2** and **3** also showed antagonistic potency at the hA_{2B} AR, but their IC_{50} values fall in the high nanomolar range (IC_{50} = 441 and 319 nM, respectively).

The thiazolopyrimidines **4** and **5**, synthetic precursors of **2** and **3**, respectively, lacking LA moiety, showed high affinity for the A_{2A} AR, were scarcely active at the hA_3 AR while showed different degrees of selectivity versus the A_1 AR subtype. The meta-substituted derivative **4** exhibited nanomolar affinity for the hA_1 AR (Ki = 26.8 nM) while the para-substituted compound **5** was 23-fold less active at A_1 AR (K_i = 662 nM) with respect to the hA_{2A} AR. Derivatives **4** and **5** showed high antagonistic potencies at the hA_{2A} AR (IC_{50} = 38.4 and 84.6 nM, respectively). Derivative **4** proved also to be active in the nM range (IC_{50} = 95.6 nM) as hA_{2B} AR antagonist, while **5** was scarcely active (IC_{50} = 1695 nM).

The antioxidant-hybridized thiazolopyrimidines **1–3**, potent hA_{2A} AR antagonists, were evaluated in LPS-stimulated BV2 microglial cells, an in vitro model of inflammation (see Section 2.6. Pharmacological studies). Derivatives **4** and **5**, lacking the LA portion, were tested to assess the contribution of the antioxidant portion in these tests.

2.3. 2,2-Diphenyl-1-picrylhydrazyl (DPPH) assay

Compound **1** was evaluated for its free radical scavenging activity (RSA) in the DPPH assay. The amine derivatives **4** and **5**, used as reference ligands in cell-based assays, were also tested to rule out any antioxidant property. In contrast, LA derivatives **2** and **3** were not tested, as the LA moiety in this form lacks reducing power and was therefore expected to be inactive [26]. The RSA was evaluated as the percentage of DPPH discoloration and plotted against compound concentration to determine steady-state inhibition (Fig. 3).

Ascorbic and gallic acids were used as reference antioxidants, and EC_{50} values (concentrations required to reduce DPPH by 50%) were calculated (Table 2). It is worth noting that catechol-containing compound **1** exhibited good RSA, exceeding that of the reference ascorbic and gallic acids. As expected, derivatives **4** and **5** were inactive (Fig. 3).

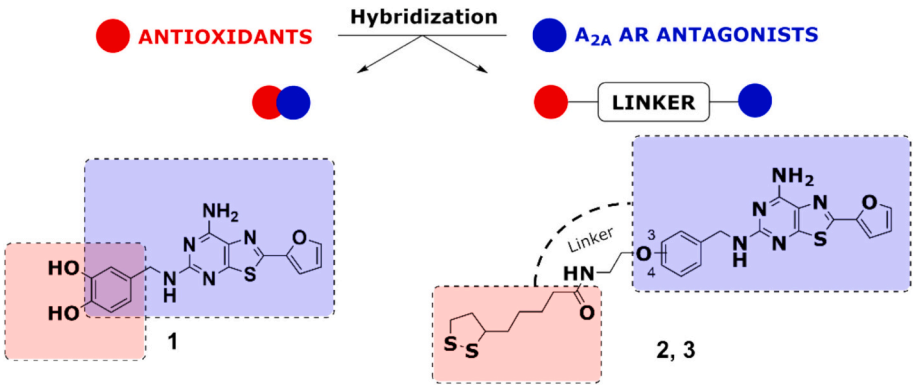

Fig. 2. Hybridization approach to obtain the desired antioxidant-based derivatives **1–3**.

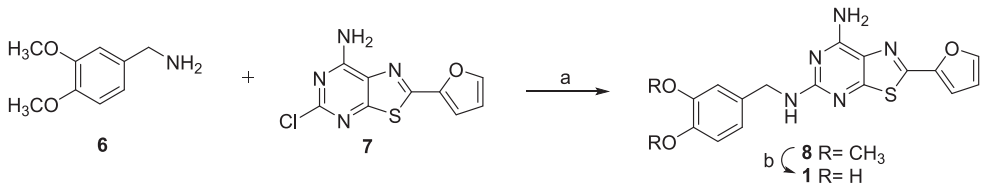

Scheme 1. Reagents and conditions: (a) n-BuOH, MW, 200 °C, 20 min; (b) BBr_3, CH_2Cl_2, 50 °C.

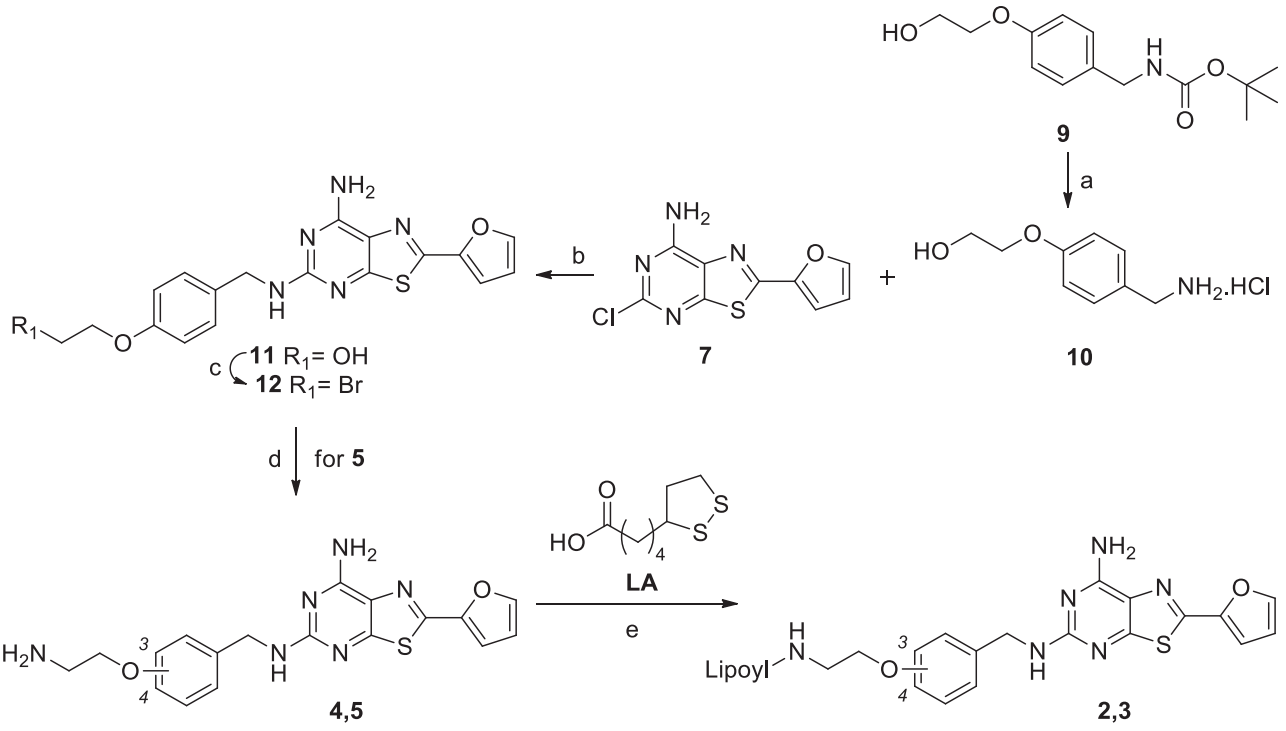

Scheme 2. Reagents and conditions: (a) 2.68 M HCl in 1,4-dioxane, 1 h; (b) n-BuOH, Et_3N, MW, 200 °C, 30 min; (c) PPh_3, N-bromosuccinimide (NBS), anhydrous CH_2Cl_2, 50 °C; (d) NH_3 gas/absolute EtOH, sealed tube, 130 °C; (e) EDCI, HOBt, Et_3N, anhydrous DMF.

Table 1
Binding and functional activity at the human adenosine receptors.[a]

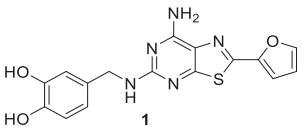

1

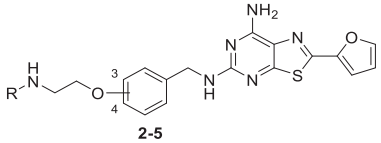

2-5

	R	Position	Binding experiments K_i (nM)			cAMP assay IC_{50} (nM)	
			hA_1[b]	hA_{2A}[c]	hA_3[d]	hA_{2A}[e]	hA_{2B}[f]
1	–	–	279 ± 24	10.1 ± 0.7	136 ± 10	22.7 ± 1.6	84.5 ± 6.1
2	Lipoyl	3	822 ± 63	16.4 ± 1.0	791 ± 58	34.1 ± 2.1	441 ± 29
3		4	2297 ± 176	39.8 ± 2.5	>10,000	101 ± 8	319 ± 24
4[g]	H	3	26.8 ± 1.9	33.9 ± 2.7	857 ± 63	38.4 ± 3.1	95.6 ± 7.4
5		4	662 ± 42	29.1 ± 2.3	1442 ± 118	84.6 ± 6.3	1695 ± 121

[a] Data (n = 3–6) are expressed as means ± SEM. Affinity values obtained from displacement of specific binding to hA_1 ARs, hA_{2A} ARs, or hA_3 ARs.
[b] Affinity values obtained from displacement of specific [^{3}H]-8-cyclopentyl-1,3-dipropylxanthine ([^{3}H]-DPCPX) binding.
[c] Affinity values obtained from displacement of specific [^{3}H]-ZM241385 binding.
[d] Affinity values obtained from displacement of specific [^{125}I]-N^6-(4-aminobenzyl)-N-methylcarboxamidoadenosine ([^{125}I]-ABMECA) binding.
[e] Potency (IC_{50}) in cAMP assays to hA_{2A} ARs.
[f] Potency (IC_{50}) in cAMP assays to hA_{2B} ARs.
[g] Reference [23].

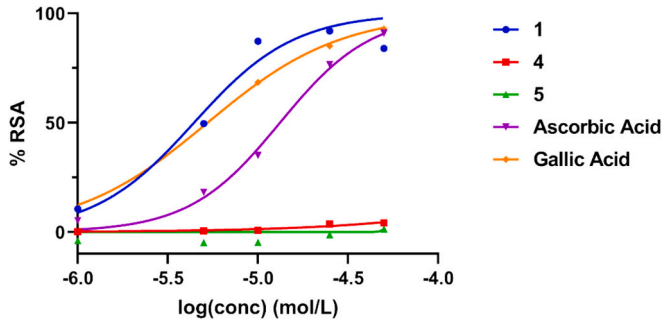

Fig. 3. Radical scavenging ability of the catechol-hybridized thiazolopyrimidines **1**, **4** and **5**.

Table 2
EC_{50} values are compound concentrations causing a 50% decrease in the DPPH absorbance.

	EC_{50} (μM)
1	4.419 ± 0.047
AA[a]	13.25 ± 0.016
GA[b]	5.251 ± 0.016

Values are mean ± SE, $n = 3$.
[a] Ascorbic Acid.
[b] Gallic Acid.

2.4. Chemical stability

Given the presence of potentially labile structural features, the chemical stability of derivatives **1–3** was assessed by monitoring (LC-MS/MS methods) the variation of their concentrations at different incubation times in 50 mM tris-(hydroxymethyl)aminomethane) hydrochloride buffer solution (Tris buffer, pH = 7.4). By plotting these data (natural logarithm of analyte concentration vs the incubation time), the respective degradation profiles were obtained (Fig. 1S–3S) which demonstrated that all the compounds were stable in 50 mM Tris buffer.

2.5. Molecular modeling studies

A molecular modeling study was performed to simulate the binding mode of the synthesized compounds at hA_{2A} AR and to rationalize A_{2A} AR affinities. The crystal structure of the antagonist-bound hA_{2A} AR (pdb code: 5NM4; 1.7-Å resolution [27]) was retrieved from the Protein Data Bank (www.rcsb.org). This structure was used as a target for molecular docking studies performed within the MOE, by using the MOE docking tool (*induced fit* docking and optimization protocol), and within CCDC Gold software (Chemscore, ASP, and PLP scoring functions) [28]. For each analyzed compound, the top-score docking pose at the hA_{2A} AR, according to at least three out of four scoring functions, was selected for final ligand-target interaction analysis.

The simulated binding mode at the hA_{2A} AR structure, generally associated to the best score, presents the thiazolopyrimidine scaffold located in the center of the hA_{2A} AR cavity, making interactions with the side chains of residues Phe168, belonging to the extracellular loop (EL) 2 segment, and $Ile249^{6.51}$. Fig. 4 represents the simulated binding mode of compound **1** taken as a reference molecule to define the position of the substituents on the thiazolopyrimidine nucleus.

The 2-furyl ring at the 2-position points toward the depth of the binding cavity, getting in proximity of residues $Leu85^{3.33}$, $Trp243^{6.48}$, and $His250^{6.50}$. The amino group at the 7-position makes polar interactions with $Asn253^{6.55}$ and Glu169 (EL2) residues, in analogy with several ligands co-crystallized with the hA_{2A} AR. The substituent at the 5-position (containing catechol system) points toward the external

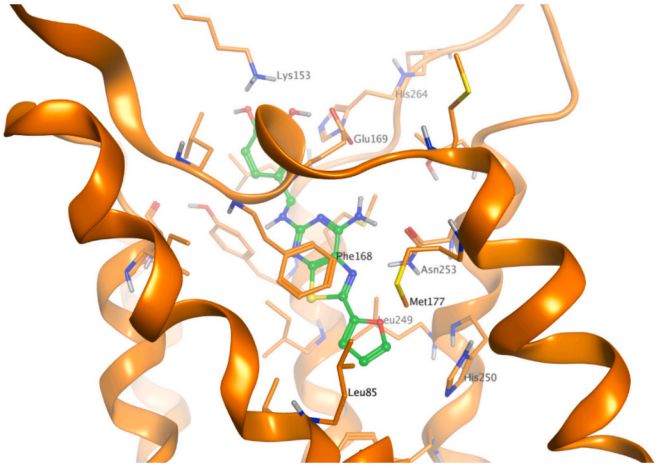

Fig. 4. Docking conformations at hA_{2A} AR. The simulated binding mode of compound **1** is shown, with detail of key receptor residues involved in ligand-target interaction.

environment, making polar interaction with residues of TM1, TM2, TM7 domains, and with the EL2 (i.e., Glu169) and EL3 segments (i.e., Lys153 and His264).

Modifications of this substituent by inserting an ethoxyamine in the meta- or the para-position of the 5-benzylamine lead to similar effects on the hA_{2A} AR affinity. Docking studies suggest that the ethoxyamine may provide an analogue interaction with the receptor due to its flexibility and limited size and a consequent ability to interact with the same amino acids of the binding cavity when inserted in the para- or meta-position. Analogous results were observed in the docking studies of compounds **2** and **3,** which bear a LA residue in the *meta-* or *para*-position of the benzylamine substituent. Fig. 5 shows the docking results at the hA_{2A} AR, highlighting once again that the flexibility of the chain may enable both compounds to establish similar interactions with the receptor, despite the different position of LA insertion. This is consistent with the comparable affinity data of the two compounds at the hA_{2A} AR,

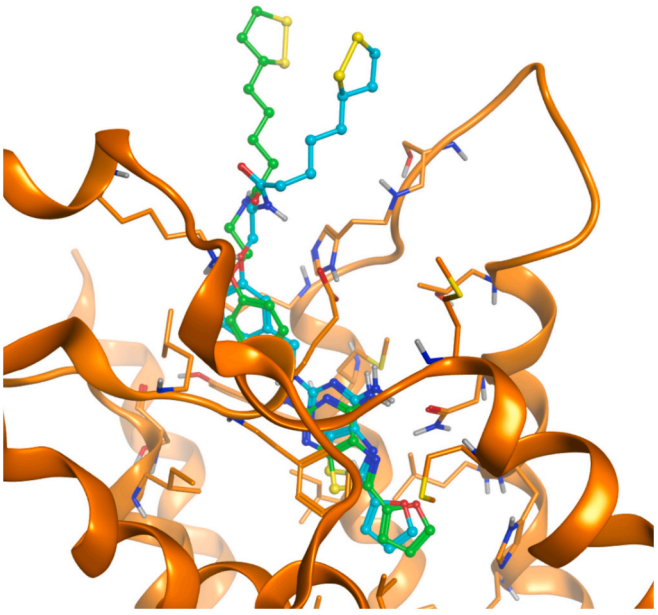

Fig. 5. Docking conformations at hA_{2A} AR. The simulated binding mode of compounds **2** (cyan) and **3** (green) is shown, with details of key receptor residues involved in ligand-target interaction. (For interpretation of the references to color in this figure legend, the reader is referred to the web version of this article.)

with compound **2** showing a slightly higher affinity.

2.6. Pharmacological studies

The thiazolopyrimidine derivatives **1–3** were tested on LPS-stimulated BV-2 microglial cells, an in vitro model of neuroinflammation and oxidative stress. It is well established that microglial activation leads to the development of inflammatory processes that, if uncontrolled, result in neuronal damage and neurodegenerative diseases [29]. This pathological response can be triggered either by activation of A_{2A}/A_{2B} ARs expressed on microglia, which initiate pro-inflammatory signaling cascades (e.g., cytokine release) [8], or by the presence of reactive species (ROS and reactive nitrogen species, RNS). Microglia sense these reactive species as indicators of cellular damage and respond by releasing pro-inflammatory cytokines (e.g., TNF-α, IL-6, interferon-γ). This process is not inherently pathological, but it becomes detrimental when the organism fails to efficiently eliminate ROS and RNS, thereby promoting sustained inflammatory responses [30].

2.6.1. Effects of synthesized compounds on cell viability and metabolic activity under basal conditions

As preliminary tests, the effect of compounds **2** and **3** on BV2 cell viability under basal conditions was assessed using the crystal violet (CV) assay. To optimize the treatment concentration, cells were exposed to different doses (from 0.001 to 1000 μM) of the compounds for 24 h. Cell viability was significantly decreased at all concentrations above 10 μM for both compounds **2** and **3** (Fig. 6A).

The IC_{50} values were calculated from the dose-response curve of nine applied concentrations from the absorbance obtained from CV assay and were 25,48 μM and 38 μM for compounds **2** and **3**, respectively (Fig. 6B). The effects of derivatives **1–3** on BV2 cell metabolic activity were evaluated using the 3-(4,5-Dimethyl-2-thiazolyl) 2,5-diphenyl-2-H-tetrazolium bromide (MTT) assay at concentration ranging from 0.001 μM to 100 μM, Also in this test, the highest compound concentration that did not affect metabolic activity was 10 μM (Fig. 7A). This result was also consistent with the cell morphology observed in bright-field micrographs (Fig. 7B). Based on these findings, in subsequent experiments on LPS-stimulated BV2 cells, the compounds were tested at a concentration of 10 μM.

2.6.2. Effect of synthesized compounds on LPS-stimulated BV2 cells

LPS-stimulated BV-2 microglial cells are characterized by increased levels of pro-inflammatory cytokines [31], inducible nitric oxide synthase (iNOS) [32] and markers of oxidative damage [33]. These cells were co-treated for 24 h with the thiazolopyrimidine derivatives **1–3** at a concentration of 10 μM. **LA** and derivatives **4** and **5** were also evaluated

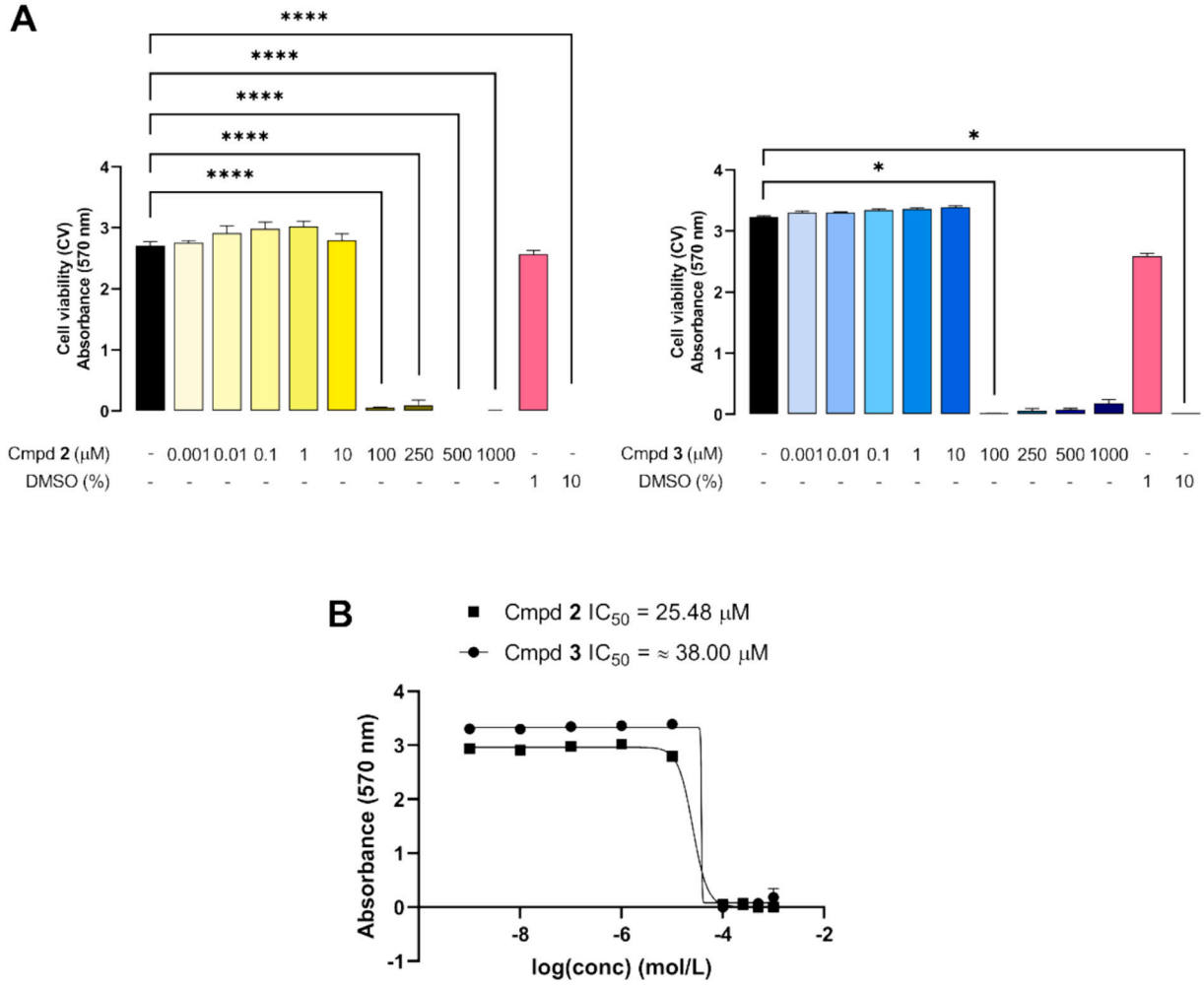

Fig. 6. Effect of compounds **2** and **3** on BV-2 viability. (A) Cell viability determined by CV assay of control and treated cells with compounds **2** and **3**, or 1 and 10% DMSO. (B) IC_{50} values for compounds **2** and **3** calculated from the dose-dependent curve of nine applied concentrations from the absorbance obtained from CV assay. The results are expressed as mean optical density (OD, 570 nm) ± SEM, from $n = 4$ independent determinations performed in duplicate and relative absorbance normalized to control ± SEM, and were analyzed by one-way ANOVA (compound **2**) or by Kruskal–Wallis test (compound **3**) followed by Tukey's or Dunn's multiple comparisons test, respectively. ****< 0.0001, *≤ 0.05 vs. control group.

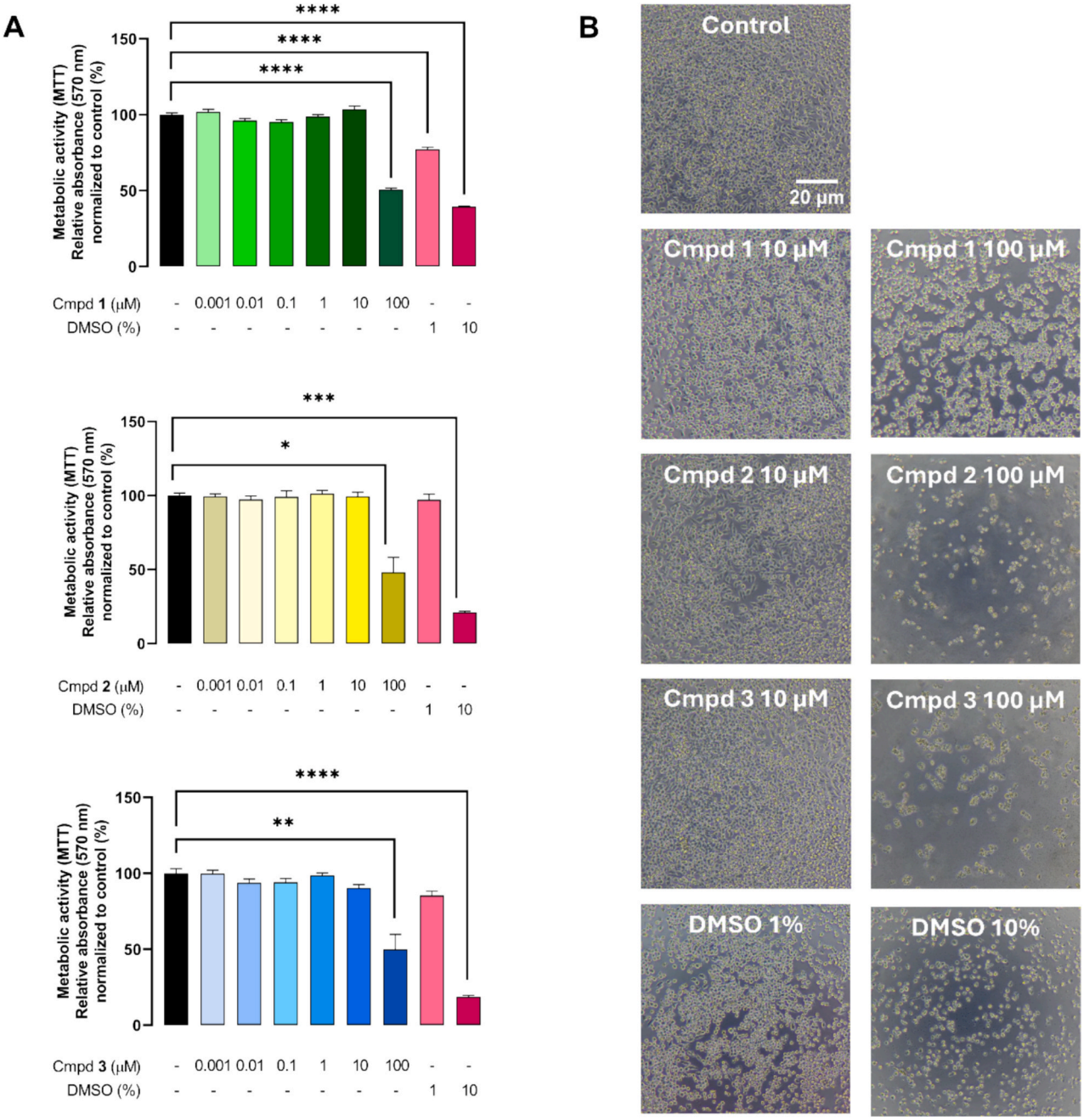

Fig. 7. Effect of compounds **1–3** on BV-2 metabolic activity. (A) Metabolic activity determined by MTT assay of control and LPS-stimulated BV-2 cells treated with compounds **1–3**, or 1 and 10% DMSO. (B) Bright-field micrographs showing the highest safe (10 μM) and the lowest harmful (100 μM) tested concentrations for compounds **1–3**. 1 and 10% DMSO were used as a reference. Frames were randomly imaged using a ZEISS Primovert inverted cell culture microscope with an Axiocam 208 color camera (Zeiss, Germany) and a 10× objective, and stored as digitalized data. The results are expressed as mean optical density (OD, 570 nm) ± SEM, from three or four independent determinations performed in duplicate and relative absorbance normalized to control ± SEM, and were analyzed by one-way ANOVA (compound **2**) or by Kruskal–Wallis test (compounds **1** and **3**) followed by Tukey's or Dunn's multiple comparisons test, respectively. **** < 0.0001, ***< 0.001, **< 0.01, * ≤ 0.05 vs. control group.

as reference ligands. The effects of the tested compounds on cell morphology, inflammatory parameters (NO production, extracellular signal-regulated kinase, and pro- and anti-inflammatory cytokines), and antioxidant factors (glutathione, malondialdehyde, superoxide anion, and enzymes catalase and superoxide dismutase) were then assessed.

2.6.2.1. Effect of synthesized compounds on LPS-stimulated cell morphology. The effect of derivatives **1–5** and **LA** on cell morphology was measured by analyzing brightfield micrographs (Fig. 8). All analyzed morphology parameters (mean area and shape descriptors) were summarized in Table 3. LPS treatment induced a significant increase in BV-2 cell area, accompanied by marked changes in shape descriptors, including increased aspect ratio and perimeter, along with reduced circularity, roundness, and solidity. Collectively these changes indicate a transition toward an activated, elongated, and less regular cellular morphology.

Among the tested compounds, thiazolopyrimidine hybrids **2** and **3**, together with thiazolopyrimidine **4** and the antioxidant **LA**, significantly reduced BV-2 cell area and perimeter. Hybrid **3** increased circularity and solidity, whereas hybrid **2** and **LA** also increased roundness, indicating a

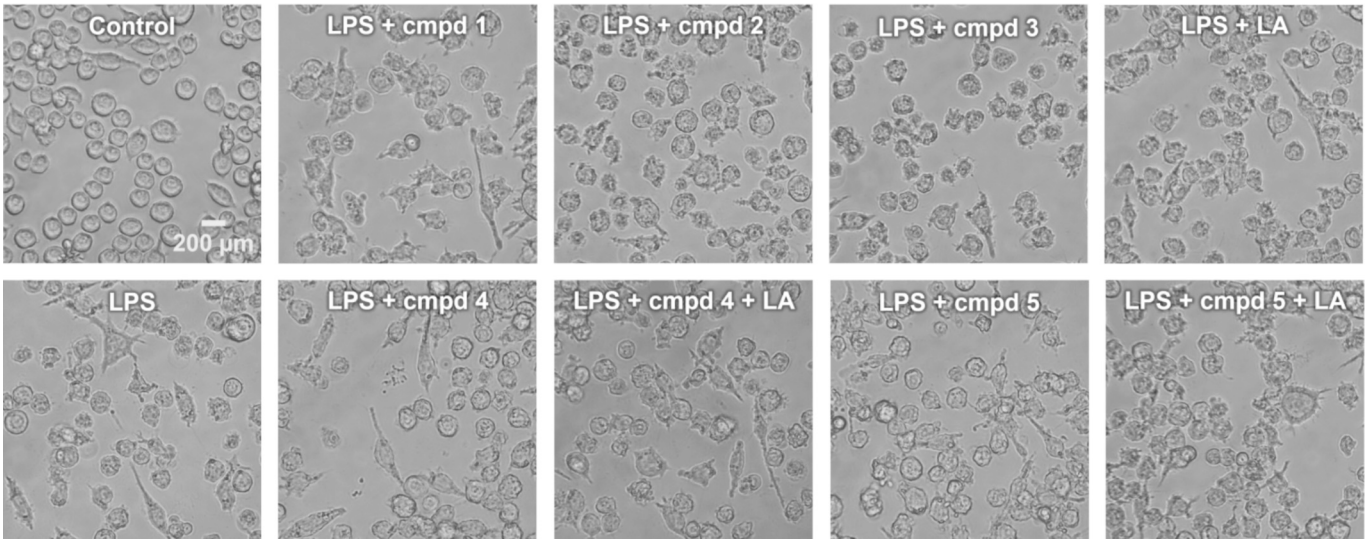

Fig. 8. Representative brightfield micrographs of untreated BV-2 cells and after 24 h of treatment with LPS (1 µg/mL) and compounds **1–5** and **LA** (10 µM). Frames were randomly imaged using a ZEISS Primovert inverted cell culture microscope with an Axiocam 208 color camera (Zeiss, Germany) and a 40× objective, and stored as digitalized data. Images were used to determine cell surface area and shape descriptors in ImageJ.

Table 3
Thiazolopyrimidine derivatives **1–5** effect on cell morphology parameters.[a]

	Area (µm^2)	Aspect ratio	Perimiter	Circularity	Roundness	Solidity
Control	231.1 ± 3.2	1.245 ± 0.02	57.24 ± 0.7	0.915 ± 0.01	0.845 ± 0.01	0.987 ± 0.00
LPS	309.6 ± 6.3$^{\#\#\#\#}$	2.163 ± 0.07$^{\#\#\#\#}$	91.95 ± 2.2$^{\#\#\#\#}$	0.594 ± 0.02$^{\#\#\#\#}$	0.589 ± 0.01$^{\#\#\#\#}$	0.857 ± 0.01$^{\#\#\#\#}$
LPS + **1**	309.6 ± 7.4	1.834 ± 0.07	86.65 ± 2.7	0.675 ± 0.02	0.672 ± 0.02	0.88 ± 0.01
LPS + **2**	251.7 ± 7.2***	1.640 ± 0.10	68.31 ± 2.6****	0.784 ± 0.02****	0.739 ± 0.02****	0.943 ± 0.01****
LPS + **3**	252.9 ± 6.7**	1.688 ± 0.09	68.78 ± 2.2***	0.770 ± 0.02***	0.704 ± 0.02	0.933 ± 0.01**
LPS + **4**	255.1 ± 8.4****	1.882 ± 0.12	75.73 ± 3.3**	0.703 ± 0.03	0.676 ± 0.02	0.905 ± 0.01
LPS + **5**	269.2 ± 6.8	1.860 ± 0.10	78.23 ± 3.5	0.692 ± 0.03	0.654 ± 0.02	0.897 ± 0.01
LPS + **4** + **LA**	289.2 ± 9.6	1.910 ± 0.13	85.78 ± 4.4	0.673 ± 0.03	0.676 ± 0.02	0.870 ± 0.02
LPS + **5** + **LA**	265.6 ± 8.3*	1.961 ± 0.11	79.24 ± 3.2	0.676 ± 0.03	0.652 ± 0.03	0.881 ± 0.01
LPS + **LA**	258.0 ± 6.7***	1.763 ± 0.07	73.53 ± 2.4***	0.761 ± 0.02****	0.695 ± 0.02***	0.925 ± 0.01****

[a] Mean area (µm^2) and shape descriptor values expressed as a mean ± SEM, from $n \geq 100$ cells in 3 random and non-overlapping microscopic fields. Data were analyzed by the Kruskal–Wallis test followed by Dunn's multiple comparisons test.
$^{\#\#\#\#}$ $p < 0.0001$ vs. control group.
* $p < 0.05$.
** $p < 0.01$.
*** $p < 0.001$.
**** $p < 0.0001$ vs. LPS group.

partial restoration of a more regular morphology. Notably, co-treatment with **LA** and thiazolopyrimidines **4** or **5** did not produce significant changes in cell morphology. In contrast, the catechol-containing hybrid **1** failed to induce an anti-inflammatory morphological profile. The ability of the LA-hybrids **2** and **3,** as well as **LA**, to reverse the pathological morphology of LPS-stimulated BV2 cells indicates suppression of LPS-induced microglial activation and attenuation of neuroinflammatory response.

2.6.2.2. Effect of synthesized compounds on NO production and phosphorylated extracellular signal-regulated kinase (pERK) pathway. NO production was analyzed using the Griess assay (Fig. 9A). The thiazolopyrimidine hybrids **1–3** significantly reduced NO production compared with LPS-stimulated cells. Interestingly, co-treatment with thiazolopyrimidines **4** or **5** and **LA** also led to a reduction in NO levels, whereas compounds **4**, **5**, or **LA** alone showed no effect. NO is known to contribute to pathological conditions, not only through its ability to generate RNS (e.g., peroxynitrite), which can damage DNA, lipids, proteins, and integrity of the blood-brain barrier (BBB), but also through its role as a cellular signaling mediator, modulating the expression of pro-inflammatory cytokines and enzymes such as cyclooxygenase-2 (COX-2) [34]. The NO reducing effects of thiazolopyrimidine derivatives are likely related to their antagonistic activity at A_{2A}/A_{2B} ARs, whose activation triggers signaling pathways that induce expression of inducible nitric oxide synthase 2 (NOS2; iNOS) and potentiate NO-mediated inflammatory responses [35], as well as to the presence of an antioxidant portion. This hypothesis is supported by the observation that compounds **1–3** produced a more pronounced reduction in NO levels, compared with the reference A_{2A} AR antagonists **4** and **5**, which lack the antioxidant portion and induced a reduction in NO levels that was not statistically significant.

Interestingly, compound **4** displayed appreciable affinity for the A_1 AR. Although the role of A_1 AR in inflammatory processes remains controversial and both pro- and anti-inflammatory actions have been reported depending on the experimental context, in microglial cells, A_1 AR activation has frequently been associated with anti-inflammatory effects [8,10,11], suggesting that the biological responses observed in the present study are more consistently explained by A_{2A} AR antagonism.

No effect was detected for **LA** alone. Nevertheless, a synergistic contribution of the antioxidant moiety can be inferred, as the combined treatment with intermediates **4** and **5** and **LA** resulted in a significant

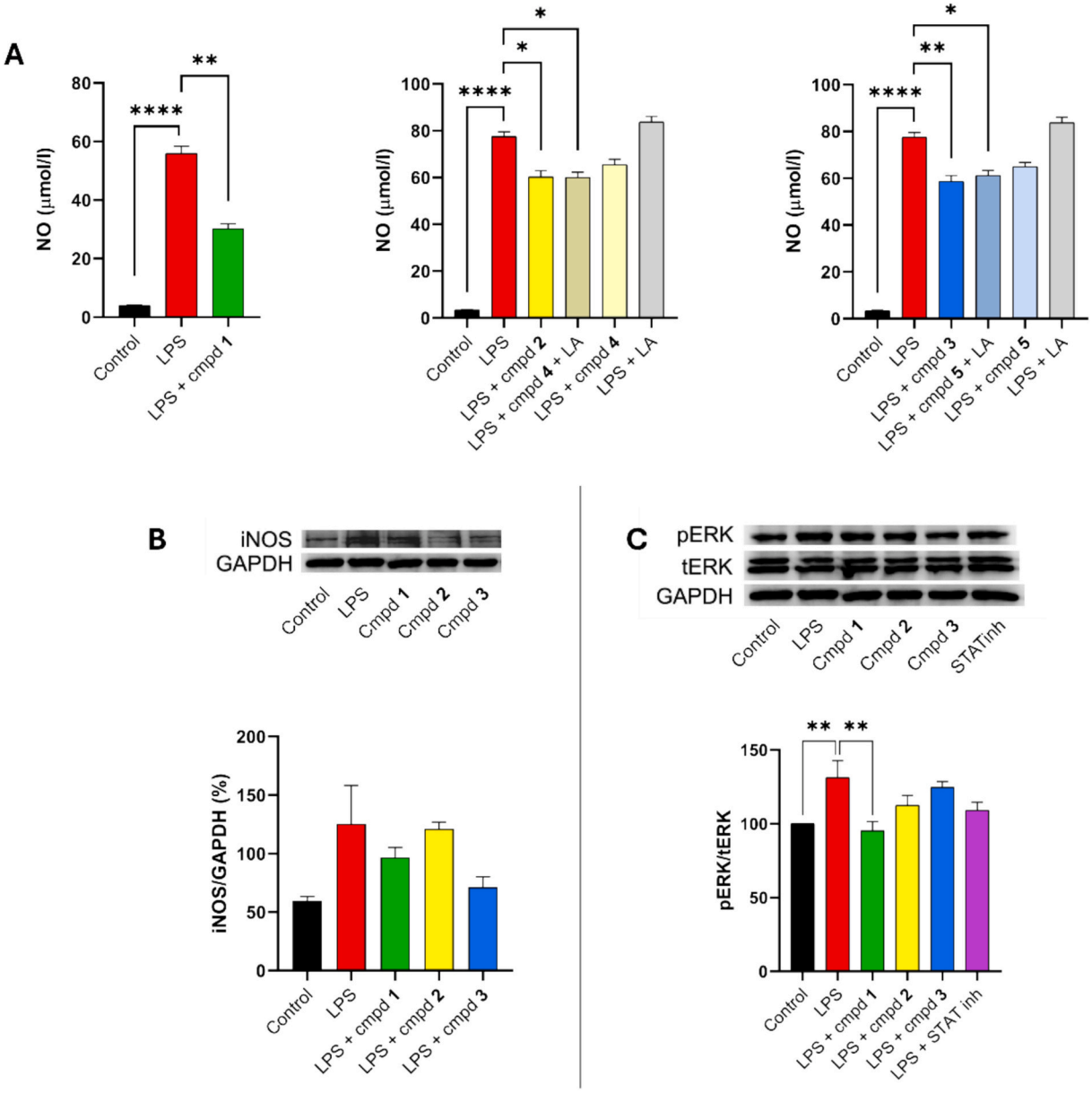

Fig. 9. Effect of thiazolopyrimidine derivatives **1–5** and **LA** on NO production. (**A**) NO accumulation in the culture medium was determined using the Griess assay as an indicator of NO release in LPS-stimulated (1 µg/mL) BV-2 treated with compounds **1–5** or **LA** (10 µM) after 24 h. (**B**) Representative immunoblot and Western Blot images showing protein levels of iNOS and (**C**) pERK in BV-2 cells LPS-stimulated (1 µg/mL) after 24 h of treatment with **1–3** or STAT inhibitor (10 µM) (used as a positive control for inhibiting ERK signaling pathway). GAPDH was used as a loading control. Data were analyzed by the Kruskal–Wallis test (NO production and iNOS expression) or by one-way ANOVA (pERK pathway activation) followed by Dunn's or Tukey's multiple comparisons test, respectively. Data are presented as mean concentration of nitrites (µM) ± SEM ($n = 3$). * $p < 0.05$, ** $p < 0.01$, **** $p < 0.0001$ vs. control or LPS group.

decrease in NO levels.

Since increased NO production during inflammation is primarily mediated by iNOS [34], we next evaluated whether iNOS expression was affected. Although no statistically significant differences were detected, a slight reduction in iNOS levels was observed after treatment with compounds **1–3**, particularly for **1** and **3** (Fig. 9B).

Given the well-established role of ERK phosphorylation in regulating iNOS expression [36], we further investigated the ability of compounds **1–3** to modulate ERK activation (Fig. 9C). ERK is activated via phosphorylation, generating phosphorylated (p) ERK, whose levels are markedly increased in microglial cells, astrocytes, and neurons [30]. At this stage, pERK contributes both to microglial activation and to the activation of inflammatory signaling pathways, leading, among other effects, to increased expression of iNOS and pro-inflammatory cytokines [36]. Moreover, A_{2A} AR can activate pERK production, further amplifying inflammatory responses [8]. Treatment of LPS-stimulated BV-2 cells with the catechol compound **1** resulted in a reduction of ERK phosphorylation, indicating anti-inflammatory activity, whereas LA derivatives **2** and **3** did not exhibit a significant effect. Since compound **1**, a dual A_{2A}/A_{2B} ARs antagonist, proved to be the most effective, the involvement of the A_{2B} AR appears to be relevant. Indeed, the A_{2B} AR is a potent activator of the MAPK/ERK pathway under inflammatory conditions, and the use of the A_{2B} AR antagonist PSB-603 has been reported to promote pERK reduction and resolution of the inflammatory process [37]. These findings suggest that the enhanced activity of compound **1** may be attributable, at least in part, to its A_{2B} AR antagonistic component.

2.6.2.3. Effect of synthesized compounds on inflammatory parameters. The ability of hybrids **1–3**, thiazolopyrimidines **4** and **5**, and **LA** to modulate the pro-inflammatory cytokines TNF-α and IL-6, as well as the anti-inflammatory cytokine Interleukin 10 (IL-10), was evaluated in both cell culture media (Fig. 10A) and cell lysates (Fig. 10B). After LPS stimulation, a consistent increase of pro-inflammatory cytokines and an unchanged level of the anti-inflammatory cytokine was observed in both compartments. The production and release of these pro-inflammatory cytokines are closely associated with pathological activation of A_{2A} AR under inflammatory conditions [38]. In contrast, stimulation of the A_{2B} AR has been reported to increase IL-6 production and to exert an anti-inflammatory effect by modulating TNF-α concentration [39]. Additionally, the use of **LA** and catechol-based compounds has been directly correlated with reduced levels of pro-inflammatory cytokines [17,40]. Although none of the tested compounds reduced the levels of TNF-α, IL-6 in cell medium was significantly decreased by catechol-containing hybrid **1** and by thiazolopyrimidines **4** and **5** or their combination with **LA** (Fig. 10A). Treatment of inflamed BV-2 cells with derivatives **1–3** did not result in a significant decrease in the pro-inflammatory cytokines TNF-α and IL-6, both in cell medium and lysates, likely due to the severe inflammatory state induced by LPS or to the relatively low concentration of the tested compounds. However, treatment with the catechol-containing hybrid **1** and the LA-containing hybrid **2** significantly increased intracellular IL-10 levels (Fig. 10B), without a corresponding increase in the culture medium.

2.6.2.4. Effect of synthesized compounds on oxidative stress parameters. The effects of thiazolopyrimidines **1–5** and **LA** on oxidative stress parameters, including malondialdehyde (MDA), glutathione (GSH), superoxide anion (O_2^-), and the antioxidant enzymes catalase (CAT) and total superoxide dismutase (tSOD), were investigated (Fig. 11). None of the tested compounds was able to reduce the oxidative stress markers MDA and O_2^-, nor to increase endogenous glutathione levels or the expression of antioxidant enzymes CAT and tSOD. Rather, the treatments appeared to exert a mild pro-oxidant effect. These findings did not reflect the potent radical-scavenging activity observed in the cell-free DPPH assay for derivative **1** (Paragraph 2.3). Its behaviour could be explained by the pro-oxidant properties of polyphenols, which are dose- and cell type-dependent, leading to the phenoxyl radical generation or ROS production in the presence of transition metals [41,42]. Notably, LPS did not significantly upregulate oxidative stress markers compared with the control group, but an increase in tSOD levels was observed.

Electron paramagnetic resonance (EPR) experiments were carried out to identify short-lived radicals formed directly within the cell culture. LPS-activated BV2 cells were additionally stimulated with phorbol 12-myristate 13-acetate (PMA), known as an accessorial boost for free radical release, but increase in total free radical content after LPS + PMA treatment was not observed after 24 h stimulation (Fig. 12A). This can be a result of constant nitrogen species formation, result of dominated NO-mediated signaling in LPS-stimulated BV2 cells, which can mask and suppress detectable ROS production [43] and already mentioned time-

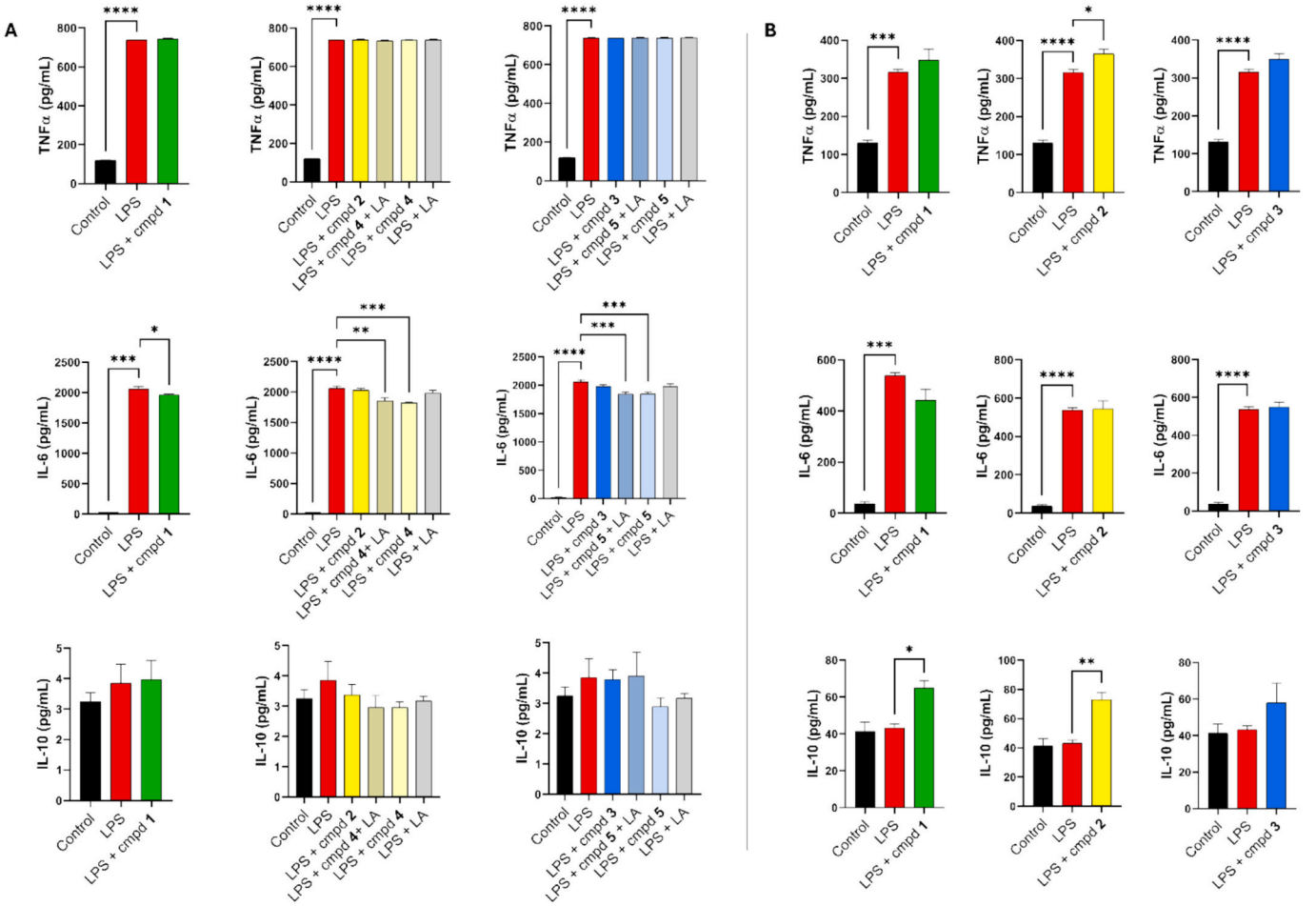

Fig. 10. Quantitative analysis of cytokine production by Enzyme-Linked Immunosorbent Assay (ELISA). The concentrations of TNF-α, IL-6, and IL-10 in cell culture mediums (A) or lysates (B) were measured using ELISA kits according to the manufacturer's instructions. Samples were analyzed after 24 h of co-treatment with LPS (1 μg/mL) and thiazolopyrimidine derivatives **1–5** and **LA** (10 μM). Results are expressed in pg/mL and represent the mean ± SEM of three independent determinations. Data were analyzed by the Kruskal–Wallis test followed by Dunn's multiple comparisons test. * $p < 0.05$, ** $p < 0.01$, *** $p < 0.001$, **** $p < 0.0001$ vs. control or LPS group.

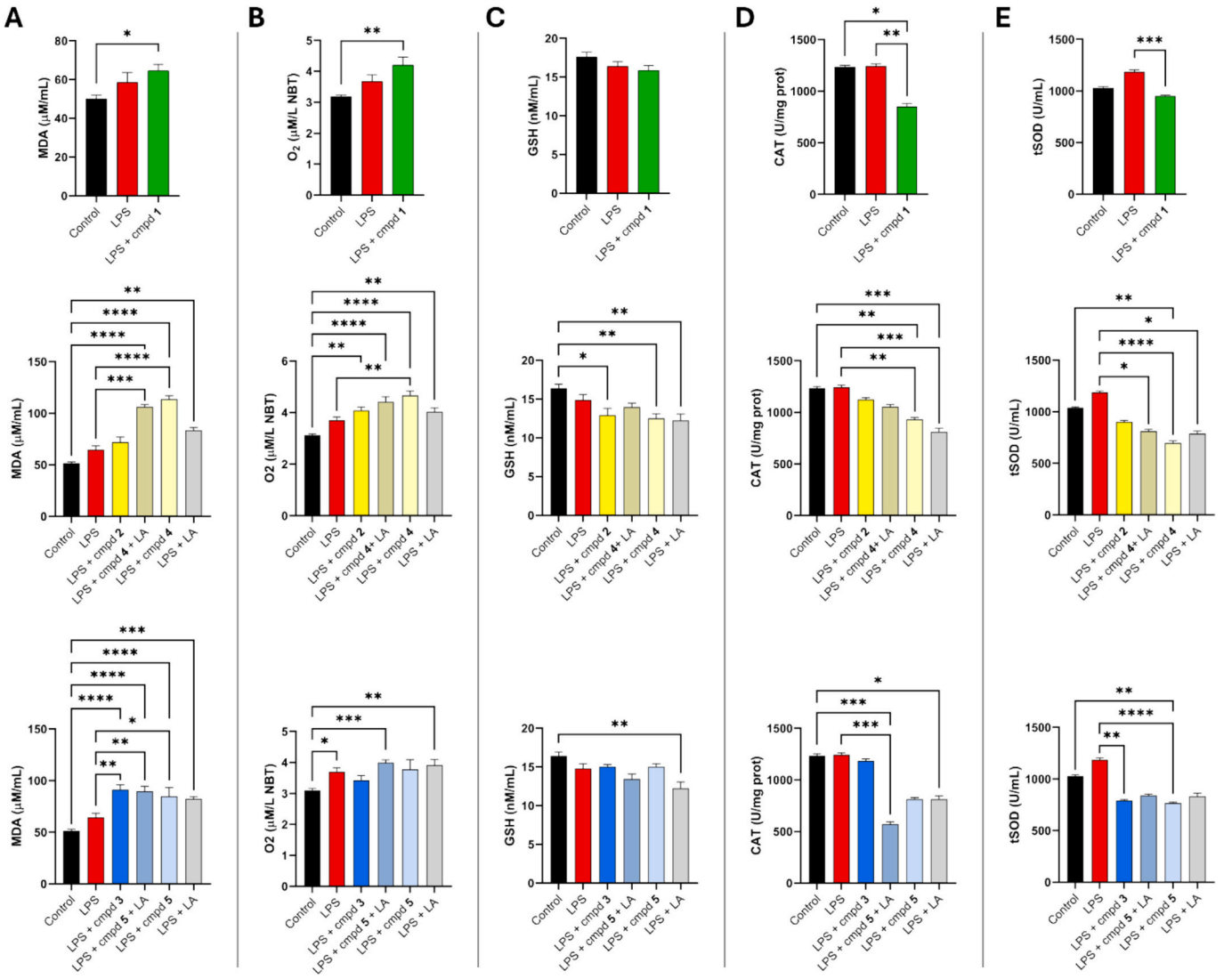

Fig. 11. Evaluation of oxidative stress markers and antioxidant status in cell lysates. BV-2 cells LPS-stimulated (1 μg/mL) were treated with thiazolopyrimidine derivatives **1–5** and **LA** (10 μM) for 24 h, and intracellular levels of oxidative parameters were measured. In particular, (A) malondialdehyde content, (B) superoxide anion production, (C) glutathione levels, and enzymatic activities of (D) Catalase and (E) total Superoxide Dismutase were assessed using colorimetric assays. All biochemical parameters were normalized to the total protein content of the lysates. Data are expressed as mean ± SEM performed in 3–5 replicates per group from three separate determinations. Data were analyzed by the Kruskal–Wallis test followed by Dunn's multiple comparisons test. * $p < 0.05$, ** $p < 0.01$, *** $p < 0.001$, **** $p < 0.0001$ vs. control or LPS group.

dependent effect since their short half-lives [44].

All tested thiazolopyrimidine hybrids (**1–3**) showed different effects on the overall free radical content (Fig. 12A), while inducing a similar trend of changes in the contribution of specific radicals. This was reflected in the decrease in hydroxyl radicals and the increase in carbon-centered (CC) radicals of about 4% for compound **2** and 10% for compounds **1** and **3**, relative to both control and LPS + PMA-treated cells, which did not significantly differ in total radical signal intensity (Fig. 12B). The lack of a significant difference between control and LPS- or LPS + PMA-treated cells does not necessarily indicate the absence of oxidative activation. Rather, it may reflect the induction of endogenous antioxidant defence mechanisms, which both decrease the steady-state levels of free radicals and promote the reduction of the formed spin adducts, ultimately leading to a diminished detectable signal. The reduction in hydroxyl radical contribution may reflect direct scavenging by the catechol or lipoic acid pharmacophores. The concomitant increase in carbon-centered radicals likely represents the formation of more stable secondary radical intermediates under specific redox conditions caused by induced stress and cellular oxidative damage. The EPR analysis may provide a further explanation for the discrepancy between cell-free and cell-based assays, as compound **1** reduced hydroxyl radical levels while simultaneously increasing carbon-centered radicals, suggesting a redistribution rather than an overall suppression of radical species.

2.6.2.5. Evaluation of blood brain barrier permeability and cellular uptake. In vitro Parallel Artificial Membrane Permeability Assay (PAMPA)-Blood Brain Barrier (BBB) assays were carried out to predict penetration of derivatives **1–5** into the brain. One of the main obstacles for the treatment of neurological diseases is the ability of drug to penetrate through the BBB at therapeutic concentrations. The BBB is a complex interface between blood and the CNS that strictly controls the exchanges between the vascular and CNS compartments [45]. This barrier is composed of endothelial cells interconnected with tight junctions that prevent the paracellular passage of endogenous materials which could damage the brain parenchyma [46]. The majority of CNS drugs enter the brain by transcellular passive diffusion, due to the tight junction structure and limited transport pathways. In early drug

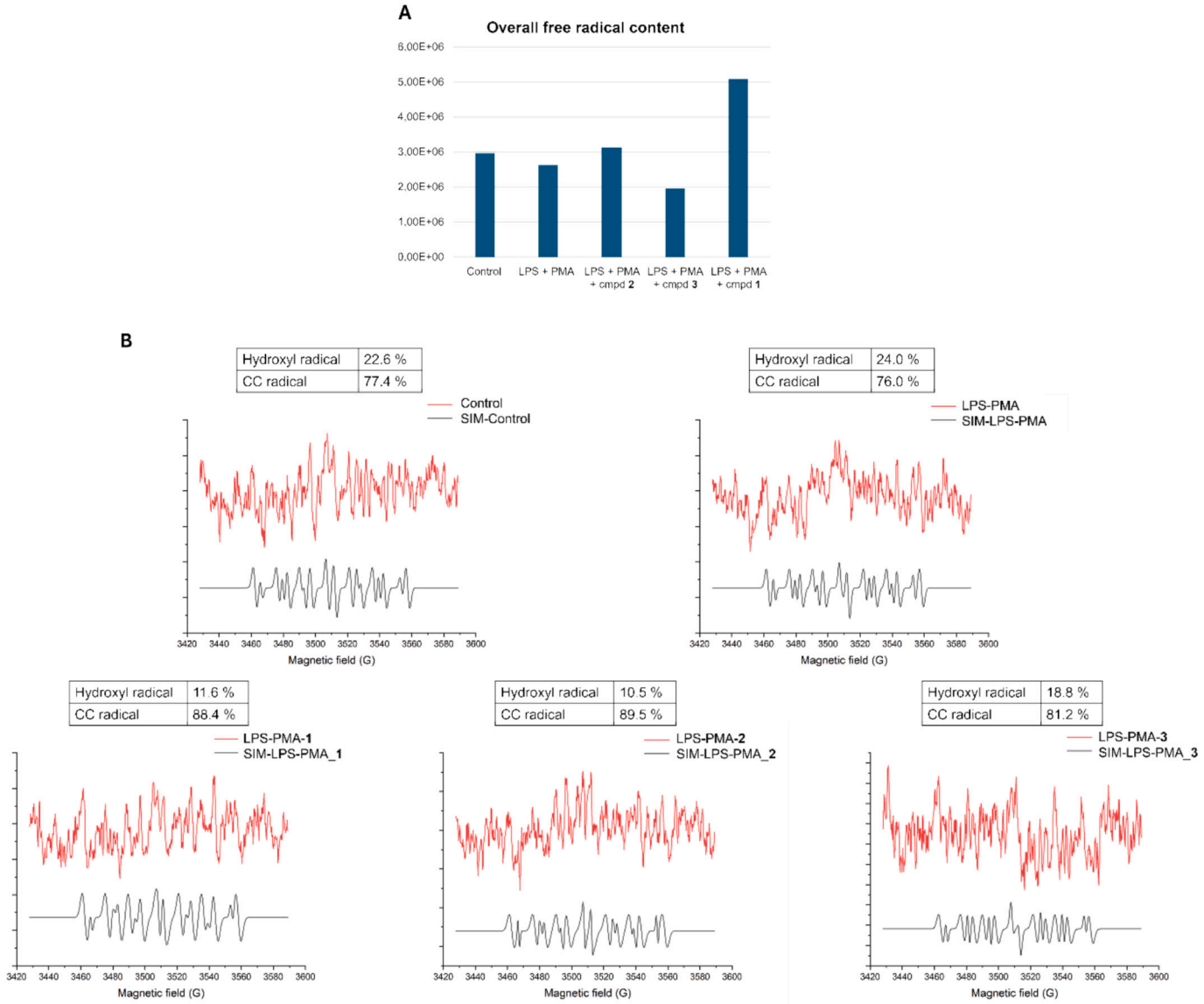

Fig. 12. EPR experiments. (A) Overall free-radical content. (B) Simulations of DEPMPO spin-adducts spectra of control, LPS-PMA stimulated and LPS-PMA stimulated BV-2 cells treated with thiazolopyrimidine hybrids **1–3** with percentage contribution of specific spin-adducts correlating to the concentration of obtained radicals. EPR simulation parameters for the DEPMPO-OH ($a^P = 46.53$ G, $a^N = 13.78$ G, $a^H[1H] = 13.35$ G), and DEPMPO-CC ($a^P = 46.74$ G, $a^N = 14.37$ G, $a^H[1H] = 21.40$ G) spin-adducts.

discovery stage, evaluation of ADME (Absorption, Distribution, Metabolism, Excretion) properties is of crucial importance to reduce attrition in development process. PAMPA is a high throughput technique developed to predict passive permeability through biological membranes. In order to explore the capacity of compounds **1–5** to penetrate into the brain, we used the PAMPA-BBB method described by Di et al. [47], which employed a brain lipid porcine membrane. The in vitro permeabilities (*Pe*) of commercial drugs through lipid membrane extract together with compounds **1–5** were determined and described in Table 4. An assay validation was made comparing the reported permeabilities values of commercial drugs with the experimental data obtained employing this methodology. A good correlation between experimental-described values was obtained *Pe* (exptl) = 1.1368 (bibl) - 0.0509 ($R^2 = 0.9525$) (Fig. 13).

From this equation and following the pattern established in the literature for BBB permeation prediction [48] we could classify compounds as CNS + when they present a permeability $>4.49 \times 10^{-6}$ cm s^{-1}. Based on these results, derivatives **1** and **2** can be predicted to cross the BBB by passive permeation (CNS+) (Table 4), a key prerequisite for CNS exposure. A similar behaviour was observed for the less lipophilic thiazolopyrimidines **4** and **5**. Compound **3** was not soluble in the assay buffer; therefore, its BBB permeability could not be determined.

While BBB permeability represents a key prerequisite for CNS exposure, pharmacological activity also requires access to target cells. Therefore, the cellular uptake of derivatives **1–3** was evaluated in BV-2 microglial cells to assess their ability to reach the intracellular site of action. To this end, the extracellular medium and the corresponding cell lysates were analyzed by HPLC–MS/MS, following incubation with the compounds. The analysis revealed a markedly higher signal intensity in the cellular fraction compared to the medium (Figs. 14–16).

In all examined cases, the chromatographic peak corresponding to the monitored compound was predominantly detected in the cell lysate, indicating preferential association of the compounds with the cellular compartment. Although the present data are semi-quantitative, the consistently stronger signal observed in the lysate suggests efficient cellular uptake and/or retention of the molecules. The washing step performed prior to cell lysis reduces the likelihood that the detected signal arises from residual extracellular compound, supporting the

Table 4
Permeability (*Pe* 10^{-6} cm s^{-1}) in the PAMPA-BBB assay for 10 commercial drugs (used in the experiment validation) and compounds **1–5** with their predictive penetration in the CNS.[a]

Compound	Bibl.[b]	*Pe* (10^{-6} cm s^{-1})[c]			Prediction
Atenolol	0.8	0.7	±	0.4	
Caffeine	1.3	0.8	±	0.2	
Desipramine	12	11.3	±	0.2	
Enoxacin	0.9	0.6	±	0.1	
Hydrocortisone	1.9	1.7	±	0.1	
Ofloxacin	0.8	0.3	±	0.1	
Piroxicam	2.5	1.2	±	0.1	
Promazine	8.8	9.6	±	0.5	
Testosterone	17	15.1	±	1.0	
Verapamil	16	11.9	±	1.3	
1		4.6	±	0.3	CNS +
2		6.3	±	0.7	CNS +
3		NT			
4		7.6	±	0.5	CNS +
5		7.6	±	0.1	CNS +

NT: not soluble in the assay buffer.
[a] PBS:DMSO (95:5) was used as solvent.
[b] Reference [47].
[c] Data are the mean ± SD of 2 independent experiments.

interpretation of a genuine cell-associated fraction. The observed intracellular enrichment suggests favorable physicochemical properties of the compounds, such as efficient membrane partitioning or interaction with intracellular components. From a pharmacological perspective, this distribution profile is consistent with a multifaceted mechanism of action of these antioxidant A_{2A}/A_{2B} adenosine receptor antagonists. In addition to modulation of receptor-mediated inflammatory pathways, compounds **1**–**3** may exert an intracellular effect contributing to their biological activity. Further quantitative studies will be necessary to determine the absolute intracellular concentrations of the derivatives.

Taken together, compounds **1** and **2** were predicted to cross the BBB, and derivatives **1–3** showed efficient uptake into BV-2 microglial cells, suggesting access to intracellular targets and thereby providing a mechanistic basis for their biologically relevant modulation of neuroinflammatory pathways, such as ERK signaling.

3. Conclusions

This work led to a set of novel thiazolopyrimidines hybridized with catechol (**1**) and **LA** (**2** and **3**). Hybrid derivatives **1–3** and synthetic intermediates **4** and **5** were identified as potent and selective A_{2A} AR antagonists, with the catechol-containing derivative **1** also antagonizing the A_{2B} AR. Docking studies highlighted key interactions of the hybrids **1–3** with the hA_{2A} AR, with the thiazolopyrimidine core interacting with Phe168 (EL2) and Ile249, the 7-amino group forming polar contacts with Asn253 and Glu169, and the flexible 5-substituent enabling comparable receptor interactions for compounds **2** and **3** despite different substitution positions. Compounds **1** and **2** were predicted to permeate the BBB, a critical requirement for molecules designed to target neurodegenerative disorders, such as MS. The catechol derivative **1** exhibited marked radical-scavenging activity in the cell-free DPPH assay, but despite this promising behaviour, neither compound **1** nor the LA-hybrid derivatives **2** and **3** were able to significantly reduce oxidative stress parameters in LPS-stimulated BV2 cells. Conversely, compounds **1–3** effectively attenuated the inflammatory response induced by LPS stimulation. In particular, hybrids **1–3** significantly decreased NO levels, while the LA derivatives **2** and **3** improved the inflammation-associated morphological alterations. Treatment with the catechol derivative **1** and the LA-containing **2** resulted in a significant increase in the production of the anti-inflammatory cytokine IL-10. The ability of derivatives **1–3** to penetrate BV-2 cells supports the hypothesis of a multifaceted mechanism of action involving both A_{2A}/A_{2B} receptor-mediated pathways and intracellular effects. Among the tested hybrids, compound **1** emerged as the most promising candidate, exhibiting functional activity through the reduction of pERK levels, thereby suppressing downstream signaling

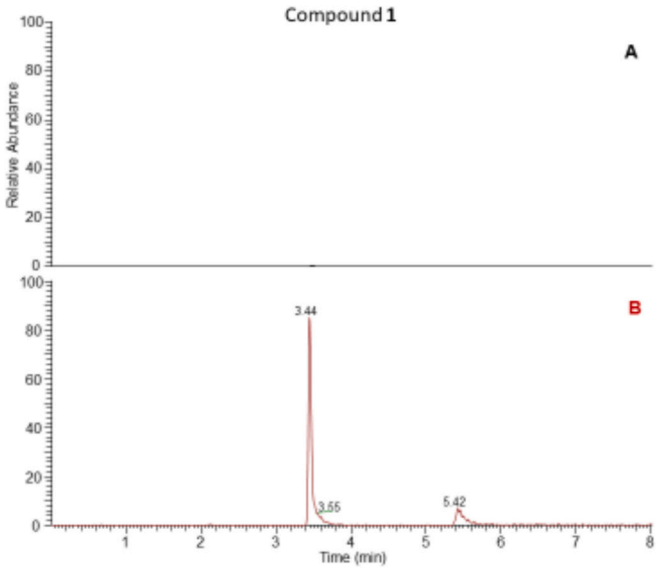

Fig. 14. Comparison of LC-MS/MS profile of derivative **1** in the medium (A) and cell lysate (B) sample.

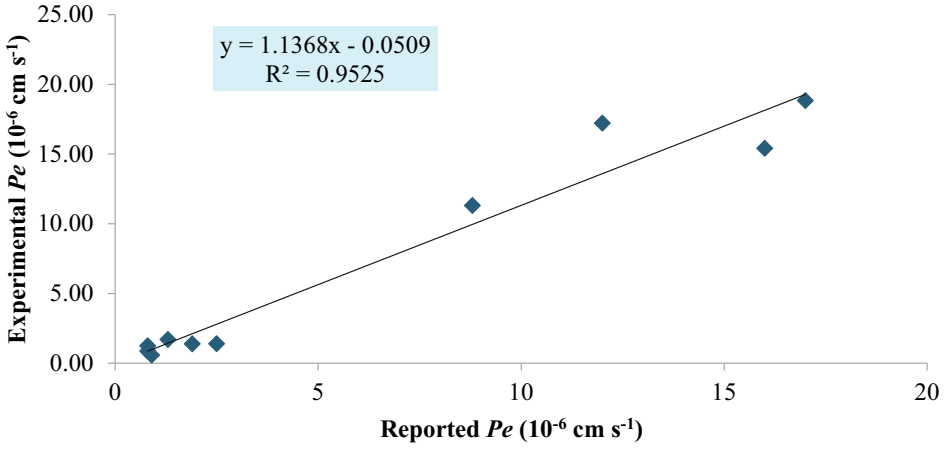

Fig. 13. Linear correlation between experimental and reported permeability of commercial drugs using the PAMPA-BBB assay.

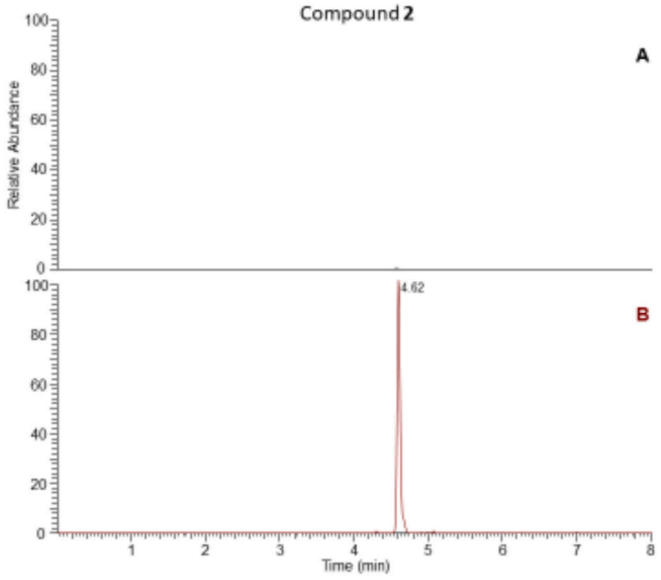

Fig. 15. Comparison of LC-MS/MS profile of derivative **2** in the medium (A) and cell lysate (B) sample.

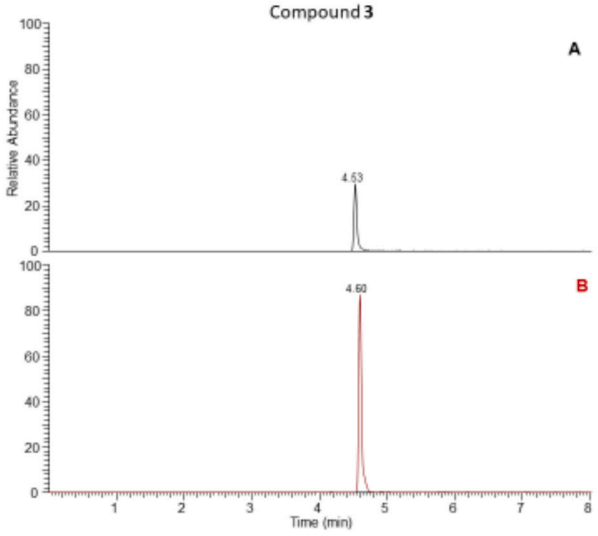

Fig. 16. Comparison of LC-MS/MS profile of derivative **3** in the medium (A) and cell lysate (B) sample.

pathway activation.

Collectively, these findings suggest that thiazolo[5,4-*d*]pyrimidine-based hybrids incorporating antioxidant moieties and exhibiting A_{2A}/A_{2B} AR antagonism may represent promising therapeutic candidates for diseases with a significant neuroinflammatory component, such as multiple sclerosis, by contributing to the reduction of inflammatory processes.

4. Experimental section

4.1. Chemistry

Analytical silica gel plates (0.20 mm, F254, Merck, Germany) and silica gel 60 (Merck, 70–230 mesh) were used for analytical and column chromatography, respectively. All melting points were determined on a Gallenkamp melting point apparatus and were uncorrected.

The high-resolution mass spectrometry (HRMS) analysis was performed with a Thermo Finnigan LTQ Orbitrap mass spectrometer coupled with an electrospray ionization source (ESI). Analysis was carried out in positive ion mode $[M + H]^+$, and it was used a proper dwell time acquisition to achieve 60,000 units of resolution at full width at half maximum (FWHM). Elemental composition of compounds was calculated based on their measured accurate masses, accepting only results with an attribution error of less than 2 ppm and a not integer RDB (double bond/ring equivalents) value. The solvents used in mass spectrometry measures were acetone, acetonitrile (Chromasolv grade), and mQ water 18 MΩ cm. Stock solutions of analytes were prepared using 25 acetone (1.0 mg/mL) and stored at 4 °C. Then, working solutions of each analyte were prepared by dilution of the stock solutions using mQ water/acetonitrile 1/1 (v/v) up to a concentration of 1.0 μg/mL. The HRMS analysis was performed by introducing the analyte working solution via syringe pump at 10 μL min^{-1}. Elemental analyses were performed with a Flash E1112 Thermofinnigan elemental analyzer for C, H, N and the results were within 0.4% of the theoretical values. Elemental analyses are reported in Supplementary Data. All compounds revealed purity not less than 95%. NMR spectra were recorded on a Bruker Avance 400 spectrometer (400 MHz for ^1H and 100 MHz for ^{13}C NMR). The chemical shifts are reported in δ (ppm) and are relative to the central peak of the solvent, which was DMSO-d_6. The following abbreviations are used: s = singlet, d = doublet, t = triplet, q = quartet, m = multiplet, brs = broad, and ar = aromatic protons. Compounds were named following IUPAC rules as applied by ChemDrawUtra 9.0. Scanned ^1H and ^{13}C NMR spectra of selected derivatives are reported in Supplementary Data.

4.1.1. 4-(((7-Amino-2-(furan-2-yl)thiazolo[5,4-d]pyrimidin-5-yl)amino)methyl)benzene-1,2-diol, 1

A solution of BBr_3 in CH_2Cl_2 (1 M, 3 mmol) was slowly added to a suspension of **8** (1 mmol) in anhydrous CH_2Cl_2 (40 mL) at 0 °C, and the mixture was refluxed for 1 h. The suspension was cooled to room temperature (rt), diluted with water (40 mL) and the mixture was stirred at rt. for 4 h, then was basified (pH 8) with an aqueous solution of $NaHCO_3$. The resulting precipitate was collected by filtration, washed with water, and purified by column chromatography (eluting system: CH_2Cl_2/MeOH 9.5:0.5). Yield 80%. Mp 226–227 °C. ^1H NMR (DMSO-d_6) 4.34 (d, 2H, CH_2, $J = 6.2$ Hz), 6.56 (dd, 1H, H ar, $J = 8.2$ Hz and $J = 1.6$ Hz), 6.64 (d, 1H, H ar, $J = 8.0$ Hz), 6.71–6.72 (m, 2H, H ar + H furyl), 7.04 (d, 1H, H furyl, $J = 3.2$ Hz), 7.14–7.18 (m, 3H, NH + NH_2, exchangeable with D_2O), 7.89 (d, 1H, H furyl, $J = 1.1$ Hz), 8.69 (brs, 2H, 2OH, exchangeable with D_2O). ^{13}C NMR (DMSO-d_6) 44.21, 109.99, 113.15, 115.09, 115.72, 118.34, 131.95, 144.32, 145.22, 145.44, 148.64, 157.50, 160.44. ESI-HRMS on $[C_{16}H_{14}N_5O_3S]^+$ species found *m/z* 256.0782. Anal. Calcd. for $C_{16}H_{13}N_5O_3S$.

4.1.2. N-(2-(3-(((7-Amino-2-(furan-2-yl)thiazolo[5,4-d]pyrimidin-5-yl)amino)methyl)phenoxy)ethyl)-5-(1,2-dithiolan-3-yl)pentanamide, 2

The thiazolopyrimidine derivative **4** (1.1 mmol) was reacted with (*R, S*) **LA** (1 mmol) in the presence of Et_3N (1.1 mmol), HOBt (1.1 mmol) and EDCI (1.1 mmol) in anhydrous DMF (2 mL) at rt. for 16 h. The mixture was diluted with water (10 mL) and extracted with EtOAc (3 × 20 mL). The organic phases were collected, washed with water (3 × 10 mL) and a saturated solution of $NaHCO_3$ (10 mL), and dried (Na_2SO_4). After elimination of the solvent under reduced pressure, **2** was obtained as a brown solid and purified by column chromatography (eluting system CHX/EtOAc/MeOH 5:5:0.1). Yield 20%. Mp 154–156 °C. ^1H NMR (DMSO-d_6) 1.29–1.37 (m, 2H), 1.47–1.57 (m, 3H), 1.59–1.68 (m, 1H), 1.78–1.86 (m, 1H), 2.08 (t, 2H, $J = 7.3$ Hz), 2.32–2.40 (m, 1H), 3.05–3.18 (m, 2H), 3.40 (q, 2H, CH_2, $J = 5.6$ Hz), 3.52–3.59 (m, 1H), 3.94 (t, 2H, CH_2, $J = 5.6$ Hz), 4.48 (d, 2H, CH_2, $J = 6.3$ Hz), 6.72 (dd, 1H, H furyl, $J = 3.5$ Hz and $J = 1.7$ Hz), 6.78 (dd, 1H, H ar, $J = 8.4$ Hz and $J = 2.0$ Hz), 6.89–6.90 (m, 2H, 2H ar), 7.05 (d, 1H, H furyl, $J = 3.4$ Hz), 7.18–7.25 (m, 3H, H ar + NH_2, exchangeable with D_2O), 7.35 (t, 1H, NH, exchangeable with D_2O, $J = 6.1$ Hz), 7.89 (d, 1H, H furyl, $J = 1.2$ Hz),

8.02 (t, 1H, NHCO, exchangeable with D_2O, J = 5.4 Hz). ^{13}C NMR (DMSO-d_6) 25.44, 28.70, 34.54, 35.53, 38.54, 38.67, 44.53, 56.56, 66.73, 110.06, 112.68, 113.16, 113.78, 119.84, 129.66, 142.89, 145.36, 148.61, 157.51, 158.92, 160.42, 172.75. ESI-HRMS on $[C_{26}H_{31}N_6O_3S_3]^+$ species found *m/z* 571.1564. Anal. Calcd. for $C_{26}H_{30}N_6O_3S_3$.

4.1.3. N-(2-(4-(((7-Amino-2-(furan-2-yl)thiazolo[5,4-d]pyrimidin-5-yl) amino)methyl)phenoxy)ethyl)-5-(1,2-dithiolan-3-yl)pentanamide, **3**

The title compound was obtained by reacting the amino derivative **5** (1.1 mmol) with (*R,S*) **LA** (1 mmol) in the same experimental conditions described above to prepare derivative **2**. The crude product was purified by column chromatography (eluting system CHX/EtOAc/MeOH 5:5:0.1). Yield 25%. Mp 160–162 °C. ^1H NMR (DMSO-d_6) 1.29–1.36 (m, 2H), 1.47–1.57 (m, 3H), 1.60–1.67 (m, 1H), 1.78–1.86 (m, 1H), 2.09 (t, 2H, J = 7.3 Hz), 2.33–2.40 (m, 1H), 3.05–3.18 (m, 2H), 3.39 (q, 2H, CH_2, J = 5.6 Hz), 3.53–3.59 (m, 1H), 3.94 (t, 2H, CH_2, J = 5.6 Hz), 4.42 (d, 2H, CH_2, J = 6.2 Hz), 6.72 (dd, 1H, H furyl, J = 3.6 Hz and J = 1.8 Hz), 6.86 (d, 2H, 2H ar, J = 8.6 Hz), 7.04 (d, 1H, H furyl, J = 3.4 Hz), 7.16 (brs, 2H, NH_2, exchangeable with D_2O), 7.23–7.30 (m, 3H, 2H ar + NH, exchangeable with D_2O), 7.88 (d, 1H, H furyl, J = 1.1 Hz), 8.01 (t, 1H, NHCO, exchangeable with D_2O, J = 5.4 Hz). ^{13}C NMR (DMSO-d_6) 25.46, 28.69, 34.54, 35.53, 38.54, 38.63, 39.40, 44.10, 56.58, 66.84, 110.03, 113.16, 114.66, 128.83, 133.26, 145.25, 148.63, 157.50, 157.64, 160.39, 172.75. ESI-HRMS on $[C_{26}H_{31}N_6O_3S_3]^+$ species found *m/z* 571.1581. Anal. Calcd. for $C_{26}H_{30}N_6O_3S_3$.

4.1.4. N^5-(4-(2-Aminoethoxy)benzyl)-2-(furan-2-yl)thiazolo[5,4-d] pyrimidine-5,7-diamine, **5**

A suspension of the bromo derivative **12** (1 mmol) in a saturated EtOH solution of NH_3 (50 mL) was heated (130 °C) in a sealed tube for 3 h. The mixture was cooled to rt., the solvent evaporated under reduced pressure, and the resulting solid was purified by column chromatography (eluting system: CH_2Cl_2/MeOH 9.5:0.5). Yield 98%. Mp 185–187 °C. ^1H NMR (DMSO-d_6) 2.83–2.85 (t, 2H, CH_2, J = 5.7 Hz), 2.86–3.90 (m, 2H, CH_2), 4.42–4.43 (d, 2H, CH_2, J = 6.1 Hz), 6.71–6.72 (m, 1H, H furyl), 6.85–6.87 (d, 2H, H ar, J = 8.2 Hz), 7.04–7.05 (m, 1H, H furyl), 7.17–7.29 (m, 5H, NH_2 + H ar + NH, exchangeable with D_2O), 7.89 (s, 1H, H furyl). ESI-HRMS on $[C_{18}H_{19}N_6O_2S]^+$ species found *m/z* 383.1264. Anal. Calcd. for $C_{18}H_{18}N_6O_2S$.

4.1.5. N^5-(3,4-Dimethoxybenzyl)-2-(furan-2-yl)thiazolo[5,4-d] pyrimidine-5,7-diamine, **8**

An excess of 3,4-dimethoxybenzilamine **6** (3 mmol) was added to a suspension of the thiazolopyrimidine **7** (1 mmol) in nBuOH (2.5 mL), and the mixture was heated at 200 °C for 30 min under microwave irradiation. The suspension was cooled to rt. and water (100 mL) was added to precipitate the desired compound **1** as a brown solid, which was collected by filtration and purified by column chromatography (eluting system: ethyl acetate/cyclohexane 4:6). Yield 50%. Mp 210–212 °C. ^1H NMR (DMSO-d_6) 3.71 (s, 3H, CH_3), 7.73 (s, 3H, CH_3), 4.42 (d, 2H, CH_2, J = 6.2 Hz), 7.2 (d, 1H, H furyl, J = 1.7 Hz), 6.85–6.88 (m, 2H, H ar), 6.99 (s, 1H, H ar), 7.04 (d, 1H, H furyl, J = 3.3 Hz), 7.18 (brs, 2H, NH_2, exchangeable with D_2O), 7.28 (s br, 1H, NH, exchangeable with D_2O), 7.89 (s, 1H, H furyl). ESI-HRMS on $[C_{18}H_{18}N_5O_3S]^+$ species found *m/z* 384.1155. Anal. Calcd. for $C_{18}H_{17}N_5O_3S$.

4.1.6. 2-(4-(Aminomethyl)phenoxy)ethan-1-ol hydrochloride, **10**

Compound **9** [25] (1 mmol) was dissolved in a 2.68 M HCl solution in dioxane (5 mmol), capped, and stirred for 1 h at rt. A precipitate formed, which was collected by filtration and used in the next step without further purification. Yield 87%. ^1H NMR (DMSO-d_6) 3.71 (t, 2H, CH_2, J = 5.1 Hz), 3.94 (q, 2H, CH_2, J = 5.8 Hz), 3.99 (t, 2H, CH_2, J = 5.1 Hz), 6.98 (d, 2H, H ar, J = 8.7 Hz), 7.40 (d, 2H, H ar, J = 8.7 Hz).

4.1.7. 2-(4-(((7-Amino-2-(furan-2-yl)thiazolo[5,4-d]pyrimidin-5-yl) amino)methyl)phenoxy)ethan-1-ol, **11**

The title compound was obtained by reacting the 7-amino-5-chloro-thiazolopyrimidine **7** (1 mmol) with the benzylamine derivative **10** (1.5 mmol) in nBuOH (2 mL) and in the presence of Et_3N (3 mmol), under the same experimental conditions described above to prepare derivative **8**. The crude product was purified by column chromatography (eluting system CH_2Cl_2/CH_3CN 8:2). Yield 68%. Mp 202–204 °C. ^1H NMR (DMSO-d_6) 3.69 (s, 2H, CH_2), 3.94 (s, 2H, CH_2), 4.42 (s, 2H, CH_2), 4.83 (s, 1H, OH, exchangeable with D_2O), 6.72 (s, 1H, H furyl), 6.86 (d, 2H, H ar, J = 7.3 Hz), 7.04 (s, 1H, H furyl), 7.17 (s, 2H, NH_2, exchangeable with D_2O), 7.24 (d, 2H, H ar, J = 7. Hz), 7.29 (s, 1H, NH, exchangeable with D_2O), 7.89 (s, 1H, H furyl).

4.1.8. N^5-(4-(2-Bromoethoxy)benzyl)-2-(furan-2-yl)thiazolo[5,4-d] pyrimidine-5,7-diamine, **12**

NBS (2 mmol) was slowly added to a cold solution of PPh_3 (2 mmol) in anhydrous CH_2Cl_2 (20 mL), keeping the temperature between −10 and 0 °C. The hydroxy derivative **11** (1 mmol) was then added in small portions and the resulting suspension was heated at reflux for 2 h. The reaction produces triphenylphosphine oxide and succinimide as by-products, which must be removed. To accomplish this, the mixture was cooled to rt. and filtered under reduced pressure to remove most of triphenylphosphine oxide. The resulting solid was resuspended in CH_2Cl_2 (30 mL) and a saturated $NaHCO_3$ solution (30 mL) was added to solubilize succinimide. The insoluble was collected and purified by column chromatography. (eluting system: CH_2Cl_2/MeOH 9:1). Yield 40%. Mp 229–230 °C. ^1H NMR (DMSO-d_6) 3.78 (t, 2H, CH_2, J = 10.8 Hz), 4.29 (t, 2H, CH_2, J = 10.8 Hz), 4.44 (d, 2H, CH_2, J = 6.3 Hz), 6.72 (m, 1H, H furyl), 6.90 (d, 2H, H ar, J = 8.5 Hz), 7.04–7.05 (m, 1H, H furyl), 7.16 (s, 2H, NH_2, exchangeable with D_2O), 7.25–7.32 (m, 3H, H furyl + H ar), 7.89 (s, 1H, H furyl).

4.2. DPPH free radical scavenging activity assay

The ability of derivatives **1, 4** and **5** to scavenge the stable free radical DPPH was assessed as previously described [21]. The assay measures the spectrophotometric change from purple to yellow that occurs when DPPH is reduced by a hydrogen-donating compound. Briefly, a solution 1×10^{-4} of DPPH in MeOH was freshly prepared and kept in the dark at rt. for 1 h before use. Then, stock solutions of **1, 4, 5**, gallic acid and ascorbic acid were prepared by dissolving compounds in DMSO to obtain a concentration of 2×10^{-4} M. Different volumes of stock solutions were diluted with MeOH to 1000 µL to obtain different molar concentrations (namely, 1×10^{-6}; 5×10^{-6}; 1×10^{-5}; 2.5×10^{-5}; 5×10^{-5}; 1×10^{-4}) and then mixed with 1000 µL of DPPH solution. The cuvettes were incubated at rt. in the dark for 30 min before measuring the absorbance at 517 nm. 2000 µL of MeOH were used as a blank. The analysis was conducted by using the UV 1900, UV-VIS Spectrofotometer Shimadzu, USA, Manufacturing Inc., Canby Oregon, USA, and the UV Transparent Disposable Cuvettes (for use from 200 nm)-Sarsted. The results are expressed as % of RSA relative to control ± Standard Error (SE), from three independent determinations.

4.3. Chemical stability

Acetonitrile (Chromasolv), formic acid and ammonium formate (MS grade), tris(hydroxymethyl)aminomethane hydrochloride (Tris HCl) were purchased by Sigma-Aldrich (Milan, Italy). The thiazolopyrimidine **11** was used as the Internal Standard (IS). Milli-Q water 18 MΩ was obtained from Millipore's Simplicity system (Milan-Italy). The 50 mM Tris buffer solution was prepared dissolving 0.8 g of tris(hydroxymethyl) aminomethane hydrochloride in 0.1 L of Milli-Q water. The analyses were carried out with a Thermo Finnigan TSQ Quantum ULTRA mass spectrometer equipped with Surveyor MS HPLC and an ESI source. Raw data was collected and processed by XCalibur 2.0. Thermostatic oven G-

Therm 015 (F.lli Galli, Milan, Italy) was used to maintain the samples at 37 °C during the stability test.

The LC-MS/MS parameters and samples preparation for each studied compound were reported in Supplementary Data.

4.4. Molecular modeling studies

Refinement of the hA_{2A} AR structure. The crystal structure of the hA_{2A} AR in complex with the antagonist ZM241385 was downloaded from the Protein Data Bank (http://www.rcsb.org; pdb code: 5NM4; 1.7-Å resolution [27]) and added of all hydrogens within the MOE (Molecular Operating Environment 2019.0101) modeling suite (Molecular Operating Environment, C.C.G., Inc., 1255 University St., Suite 1600, Montreal, Quebec, Canada, H3B 3 × 3).

Molecular docking analysis. All compound structures were subjected to docking analysis into the binding site of the hA_{2A} AR by using the Induced Fit docking protocol of MOE and the genetic algorithm docking tool of CCDC Gold [28]. The Induced Fit docking protocol of MOE is divided into a series of stages, consisting in a conformational analysis of the ligands (sistematic search protocol), placement of the generated poses within the binding site, scoring (*Alpha HB* scoring function was employed in this work) to select the best 50 poses for each ligand, energy minimization of the selected poses together with the protein sidechains in proximity to the ligands, final rescoring (*Alpha HB* scoring function). Gold docking tool was used with default efficiency settings, by selecting Chemscore, ASP, and PLP scoring functions. For each analyzed compound, the top-score docking pose at the hA_{2A} AR, according to at least three out of four scoring functions, was selected for final ligand-target interaction analysis.

4.5. Pharmacology

4.5.1. Binding and cAMP assays

4.5.1.1. Cell culture and membrane preparation. CHO cells transfected with hA_1, hA_{2A}, hA_{2B} and hA_3 ARs were grown adherently and maintained in Dulbecco's modified Eagle's medium with nutrient mixture F12, containing 10% fetal calf serum, penicillin (100 U/mL), streptomycin (100 μg/mL), L-glutamine (2 mM), geneticin (G418; 0.2 mg/mL) at 37 °C in 5% CO_2/95% air. For membrane preparation, the cells were washed with phosphate-buffered saline and scraped off T75 flasks in ice-cold hypotonic buffer (5 mM Tris-HCl, 1 mM EDTA, pH 7.4). The cell suspensions were homogenized with a Polytron, centrifuged for 30 min at 40000*g* at 4 °C and the resulting membrane pellets were used for competition binding experiments [49].

4.5.1.2. Competition binding experiments. All synthesized compounds were tested for their affinity to hA_1, hA_{2A} and hA_3 ARs. Competition experiments to hA_1 ARs were performed by incubating 1 nM [^{3}H]-DPCPX with membrane suspension (50 μg of protein/100 μL) and different concentrations of the examined compounds at 25 °C for 90 min in 50 mM TrisHCl, pH 7.4. Non-specific binding was defined as binding in the presence of 1 μM DPCPX and was always <10% of the total binding [49]. Inhibition experiments to hA_{2A} ARs were performed by incubating 1 nM of [^{3}H]-ZM241385 with the membrane suspension (50 μg of protein/100 μL) and different concentrations of the examined compounds for 60 min at 4 °C in 50 mM Tris-HCl (pH 7.4), 10 mM $MgCl_2$. Non-specific binding was evaluated in the presence of 1 μM ZM241385 and was about 20% of the total binding [50]. Competition binding experiments to A_3 ARs were carried out by incubating the membrane suspension (50 μg of protein/100 μL) with 0.5 nM [^{125}I]-ABMECA in the presence of different concentrations of the examined compounds for an incubation time of 120 min at 4 °C in 50 mM Tris-HCl (pH 7.4), 10 mM $MgCl_2$, 1 mM EDTA. Non-specific binding was defined as binding in the presence of 1 μM ABMECA and was always <10% of the total binding [51]. Bound and free radioactivity were separated by filtering the assay mixture through Whatman GF/B glass fiber filters using a Brandel cell harvester (Brandel Instruments, Unterföhring, Germany). The filter-bound radioactivity was counted in a Packard Tri Carb 2810 TR scintillation counter (Perkin Elmer).

4.5.1.3. Cyclic AMP assays. CHO cells transfected with hAR subtypes were washed with phosphate-buffered saline, detached with trypsin and centrifuged for 10 min at 200*g*. Cells were seeded in a 96-well white half-area microplate (Perkin Elmer, Boston, USA) in a stimulation buffer composed of Hank Balanced Salt Solution, 5 mM HEPES, 0.5 mM Ro 20-1724, 0.1% BSA, and 1 IU/mL adenosine deaminase. cAMP levels were then quantified by using the AlphaScreen cAMP Detection Kit (Perkin Elmer, Boston, USA) following the manufacturer's instructions [52]. At the end of the experiments, plates were read with the Perkin Elmer EnSight Multimode Plate Reader.

4.5.1.4. Data analysis. The protein concentration was determined according to a Bio-Rad method with bovine albumin as a standard reference. Inhibitory binding constant (K_i) values were calculated from those of IC_{50} according to the Cheng & Prusoff equation $K_i = IC_{50}/(1 + [C^*]/K_D^*)$, where [C*] is the concentration of the radioligand and K_D* its dissociation constant [51]. K_i and IC_{50} values were calculated by non-linear regression analysis using the equation for a sigmoid concentration-response curve (Graph-PAD Prism, San Diego, CA, USA).

4.5.2. BV2 Cell cultures

The effect of synthesized compounds was investigated on murine microglial BV-2 cell line (Elabscience Biotechnology Inc. Houston, TX, USA, Cat. No. EP-CL-0493). Cells were cultured in RPMI medium (Sigma Aldrich, Germany) with 10% heat-inactivated fetal bovine serum (Gibco, USA) and 1% penicillin/streptomycin (Gibco, USA) at 37 °C in a humidified incubator with 5% CO_2. Upon confluence, cells were collected with 0.25% trypsin (Sigma Aldrich, Germany) and 0.02% EDTA (Sigma Aldrich, Germany) in phosphate saline buffer (PBS), centrifuged (300×*g* for 5 min), counted and seeded in different cell culture dishes, depending on the experiment. For each experiment, we thawed a minimum of 3 aliquots of cells ($n \geq 3$) from different passages.

4.5.2.1. Drugs and treatments. Antagonists **1–5** were dissolved in DMSO to obtain 100 mM and 10 mM stock solutions, while **LA** was dissolved in MeOH to obtain a 100 mM stock solution. The stocks were adjusted so that the highest antagonist concentration used in the treatment (1 mM for CV assay and 100 μM for MTT) contained 1% DMSO, reported not to affect BV2 cell line [53], while 10% DMSO was used as a positive control. The maximum concentration of MeOH for **LA** dissolution was chosen so that during **LA** treatment it does not affect cell viability [54]. To optimize the concentration of compounds, cells were first treated with compounds **2** and **3** in the range of 1×10^{-9} M to 1×10^{-3} M. In further experiments, to examine the effect of the synthesized compounds on LPS-stimulated BV2 microglia, **LPS** (1 μg/mL) stimulated cells were simultaneously exposed to antagonists **1–5** (10 μM) or **LA** (10 μM) or a mixture of **4** or **5** and **LA** (10 μM) for 24 h.

4.5.2.2. Bright field microscopy and cell morphology quantification. After the treatments, the cells were washed three times with warm PBS, and ten to fifteen frames per dish were randomly imaged on ZEISS Primovert inverted cell culture microscope with Axiocam 208 color camera (Zeiss, Germany) with 10 × or 40 × objectives and stored as digitalized data. For quantification of cell morphology, cells on the micrographs were framed and cell morphology parameters (i.e., area, aspect ratio, circularity, perimeter, round, and solidity) were calculated in ImageJ/FIJI program (NIH, Bethesda, USA). Data were expressed as mean ± SEM from 100 random images per treatment, in $n = 3$ independent culture preparations.

4.5.2.3. CV assay and IC_{50} determination. For CV assay, cells were seeded in PLO (50 μg/mL, Sigma Aldrich, Germany)-coated 96-well plates (1.5×10^4 cells/well). After the treatment, cell viability was tested using CV assay. The media was discarded and the cells were washed with PBS, fixed by incubating with 4% paraformaldehyde (Sigma Aldrich, Germany) for 20 min at rt. Cells were rewashed with PBS, and 50 μL of 0.5% CV (Fluka Analytical, Switzerland) dissolved in mixture of water and methanol (75:25, *v*/v) was added to each well and incubated for 20 min at rt. Unbound CV was disposed of, and subsequent rinsing was conducted with water until a clear stream was obtained. Plates were dried at 45 °C for 1 h, then crystals were dissolved in 50 μL of glacial acetic acid, and the absorbance was measured at a wavelength of 570 nm with a microplate reader (BioTek Epoch Microplate Spectrophotometer, USA). The results are expressed as mean optical density (OD 570 nm) ± SEM, from $n = 4$ independent determinations performed in duplicate.

4.5.2.4. MTT assay. For MTT assay cells were grown in 48-well plates (5×10^4 cells/well). After the treatment, cell metabolic activity was tested using MTT assay. Medium was eliminated, and the BV2 cells were incubated with 0.5 mg/mL MTT (Sigma-Aldrich, Germany) in RPMI medium for 15 min at 37 °C. Purple crystals of formazan were dissolved in DMSO. Samples (100 μL per well) were transferred to a 96-well plate, and absorbance was measured at 570 nm with a microplate reader (BioTek Epoch Microplate Spectrophotometer, USA). The results are expressed as relative absorbance (OD 570 nm) normalized to control ± SEM, from $n = 3$ independent determinations performed in duplicate.

4.5.2.5. Measurement of NO production. Medium of the cells grown on 6-well plates (6×10^5 cells /well) was collected and frozen at −80 °C. NO in cell medium was measured using Griess assay. Griess reagent was made by mixing two solutions (1:1) right before starting the assay. Solution A was made by dissolving 1% sulfanilamide in 5% conc. H_3PO_4. Solution B is obtained by dissolving 0.1% N-(1-naphthyl) ethylenediamine dihydrochloride in distilled water. A standard curve with known concentrations of sodium nitrite (80, 40, 30, 20, 10, and 5 μM) was needed to determine the concentration of nitrites released in the sample medium. Medium samples (50 μL) were added to a 96-well plate in quintuplicate, 50 μL of the Griess reagent was added in each well, and the absorbance was measured at 540 nm (BioTek Epoch Microplate Spectrophotometer, USA). Results are expressed as mean concentration of nitrites (μM) ± SEM, from n = 3 separate determinations.

*4.5.2.6. Cellular uptake of derivatives **1–3** in BV-2 cells.* Cells were grown in 6-well plates and treated as previously described in Paragraph 4.5.2.1. The culture medium was collected and stored at −80 °C, while the cells were washed three times with PBS and subsequently lysed by scraping in cold PBS, followed by sonication on ice and storage at −80 °C. Subsequently, 0.1 mL of medium or of cell lysates were added to eppendof tube with 0.25 mL of acetonitrile, inducing protein denaturation and precipitation, then the samples were centrifuged for 3 min at 10000 rpm and the supernatants were transferred to autosampler vials and diluted with 0.15 mL of mQ water. The resulting samples were analyzed by HPLC–MS/MS to determine the extracellular and intracellular distribution of compounds **1–3**, as described in the Supplementary Data.

4.5.2.7. Western Blot analysis. BV2 microglial cells were seeded in 35 mm diameter petri dishes (6×10^5 cells/ well) and treated simultaneously with **1–3** or STAT inhibitor (10 μM) (used as positive control for inhibiting ERK signaling pathway) and LPS (1 μg/mL) for 24 h. After the treatment, culture medium was collected, and after washing in PBS, cell lysis was performed with RIPA buffer (50 mM Tris-HCl, 150 mM NaCl, 1% NP 40, 0.1% SDS, 10 mM EDTA, 10 mM EGTA, 0.5% Triton X-100, pH 7.4) with added SIGMAFAST™ Protease Inhibitor Tablets (Sigma-Aldrich, Germany). Protein concentration was measured using Pierce™ BCA protein assay kit (Thermo Fisher Scientific, USA), and the samples were adjusted to 1 mg/mL by diluting with 6 x Leamli sample buffer (375 mM Tris-HCl, pH 6.8, 12% sodium dodecyl sulfate (SDS), 60% (*w*/*v*) glycerol, 0.03% bromophenol blue). Protein denaturation was obtained by boiling the samples at 95 °C for 5 min. Proteins were separated using electrophoresis on 10% SDS polyacrylamide gel in electrophoresis system (Mini-PROTEAN III Electrophoresis Cell, Bio-Rad, USA) and transferred onto the membrane (Immobilon-P transfer membrane, Millipore) in transfer system (Bio-Rad Laboratories, USA). After blocking with 5% BSA (Sigma-Aldrich, USA) in Tris-buffer saline/Tween 20 (TBST), the membrane was incubated overnight at 4 °C with the primary antibody (Table 5). Then, the support membrane was washed 3 × 10 min in TBST and incubated for two hours at rt. with the secondary antibody (Table 5). After washing the membrane in TBST (5 × 10 min) again, the presence of target protein was detected by using a peroxide reagent and luminol-containing solution (Bio-Rad Clarity Western ECL substrate), and the protein bands were visualized using chemiluminescence ChemiDoc-It®2510 Imaging System (UVP, Upland, CA, USA). ImageJ/FIJI software package (NIH, Bethesda, USA) was used to determine relative chemiluminescence intensity. The OD of the pERK band in each lane was normalized for the OD of the total ERK band, detected on the same membrane after stripping with Mild stripping buffer (1.5% glycine, 1% SDS, 1% Tween-20, pH 2.2), while iNOS bands were normalized to GAPDH as a control protein. The results were expressed relative to the value obtained for control, arbitrarily defined as 100% (±SEM), from $n = 3$ performed in three independent experiments in duplicate.

4.5.2.8. ELISA. ELISA was used for the measurement of inflammatory cytokines (IL-6, TNF-α, IL-10) in cell medium and cell lysates. For ELISA, cells were seeded in 6-well plates (6×10^5 cells/well). After the treatment, cell medium and lysates were collected according to ELISA kit manufacturer's instructions. Briefly, cell medium was collected and centrifuged for 20 min at 1000×*g* at 4 °C before conducting the experiment. For preparing cell lysates, cells were washed twice with warm PBS, detached by adding 400 μL of 0.25% trypsin (Sigma Aldrich, Germany) and 0.02% EDTA (Sigma Aldrich, Germany) in PBS, and centrifuged for 5 min at 1000 x*g*. Supernatant was discarded, and cells were first washed three times and then resuspended in cold PBS. To obtain cell lysates, the cells were freeze-thawed three times, and, after centrifugation for 10 min at 4 °C at 1.5×10^3×g, the supernatant was collected. Prepared samples were frozen at −20 °C until the experiments. Concentration of inflammatory cytokines in prepared cell medium and cell lysates was measured by ELISA kits (Elabscience, China) according to the manufacturer's instructions - Mouse IL-6 ELISA kit (Cat. No. *E*-EL-M0044), Mouse TNF-α ELISA kit (Cat. No. E-EL-M3063) and Mouse IL-10 ELISA Kit (Cat. No. E-EL-M0046). Data are expressed as mean ± SEM from n = 3 separate determinations.

4.5.2.9. Oxidative stress parameters. BV2 cells (600,000 cells/ well) were seeded in 35 mm diameter petri dishes and treated as described.

Table 5
Antibodies used in Western Blot experiments.

Antibody	Dilution	Manufacturer
Phospho-p44/42 MAPK (Erk1/2) (Thr202/Tyr204) Antibody	1:1000 in TBST	Cell Signaling, Cat# 9101
Goat Anti-Rabbit IgG H&L (HRP), ab6721	1:30,000 in TBST	Abcam, ab6721
p44/42 MAPK (Erk1/2) Antibody #9102	1:1000 in TBST	Cell Signaling, Cat# 9102
GAPDH Polyclonal Antibody	1:2000 in TBST	ThermoFisher Scientific, PA1-987
iNOS Polyclonal Antibody	1:300 in TBST	ThermoFisher Scientific, PA1-036

After collecting the media, cells were scraped in cold PBS and sonicated on ice (each sample 3 × 10 s at 10 kHz, Bandelin Sonopuls HD 2070, Berlin, Germany). The protein concentration was determined by using the Pierce™ BCA protein assay kit (Thermo Fisher Scientific, USA) and adjusted to 1 mg/mL by diluting with PBS. Data collected from all assays are presented as mean ± SEM, performed in 3–5 replicates per group from three separate determinations.

4.5.2.9.1. MDA determination. MDA, a lipid peroxidation marker, was quantified by exploiting the red coloration of the product formed following incubation with the thiobarbituric acid (TBA) reagent (15% trichloroacetic acid and 0.375% TBA in aqueous solution, pH 3.5) at 95 °C [55]. Absorbance was recorded at 532 nm. Data are reported as mean MDA concentrations (nmol/L) ± SEM from three independent experiments performed in duplicate.

4.5.2.9.2. O_2^- determination. The content of the O_2^-radical was determined by quantifying the yellow monoformazan, the reduction product of the nitroblue-tetrazolium (NBT, Merck, Darmstadt, Germany) in an alkaline nitrogen-saturated medium, by O_2^- [56]. Kinetic was performed at 550 nm on Ultrospec 2000 spectrophotometer. The results were expressed as nmol red NBT/min/ mg protein.

4.5.2.9.3. GSH content determination. Intracellular levels of GSH were determined by using the 5,5-dithiobis-2-nitrobenzoic acid – oxidized glutathione recyclable method [57]. The content of total GSH was proportional to the level of produced yellow 5-thio-2-nitrobenzoic acid, measurable at 412 nm. Concentrations of GSH are expressed as nmol GSH/mg protein.

4.5.2.9.4. tSOD determination. tSOD activity is a combination of mitochondrial MnSOD and cytoplasmatic CuZnSOD. Its determination exploited the ability of SOD to inhibit spontaneous epinephrine auto-oxidation at alkaline pH, which leads to the pink-colored adrenochrome detectable spectrophotometrically at 480 nm [58]. Briefly, the kinetic activity was monitored in 50 mM carbonate buffer (pH 10.2) containing 1 mM EDTA following the addition of 10 mM epinephrine and 5 mM KCN for MnSOD measurement. CuZnSOD activity was calculated as the difference between tSOD and MnSOD activities. One unit is defined as the amount of enzyme required to inhibit 50% of epinephrine autooxidation, then normalized to protein content (U/mg).

4.5.2.9.5. CAT determination. A spectrophotometric method was used to determine CAT activity, leveraging the formation of the stable yellow complex produced by using ammonium molybdate and H_2O_2, detectable at 405 nm [59]. Kinetic was performed on Ultrospec 2000 spectrophotometer, and CAT activity was expressed as mmol H_2O_2 reduced per minute (mmol H_2O_2/min), (U/mg protein).

4.5.3. EPR measurements

BV2 microglial cells, seeded and maintained in 35 mm Ø Petri dishes (6×10^5 cells/ well) overnight, were trypsinized, centrifugated and resuspended in 29 μL of RPMI containing **1–3** (10 μM), LPS (1 μg/mL), and PMA (2 μM) in 1.5 mL vials that were kept in the incubator for 24 h [60]. Cells were cultured in RPMI medium (Sigma Aldrich, Germany) without 10% heat-inactivated fetal bovine serum (Gibco, USA) and 1% penicillin/streptomycin (Gibco, USA). The EPR spin-trapping technique was used to detect short-lived radicals generated directly in the cell culture. The area under the simulated 5-(diethoxyphosphoryl)-5-methyl-1-pyrroline-*N*-oxide (DEPMPO) radical adduct signal was quantified to assess its interaction with catechol or LA moieties. Briefly, 29 μL of cell culture was mixed with 1 μL of 100 mM DEPMPO. The reaction mixture was transferred into a 1 mm-diameter Teflon tube, and EPR spectra were acquired 2 min upon the addition of DEPMPO [61]. EPR measurements were conducted using a Bruker ELEXSYS II spectrometer operating in X-band at a microwave frequency of 9.8 GHz. Acquisition parameters were as follows: microwave power 10 mW, modulation frequency 100 kHz, and modulation amplitude 2 G. Simulations of the EPR spectra were carried out with SpinFit (Bruker BioSpin).

4.5.4. CNS penetration: In vitro PAMPA-BBB

Prediction of the brain penetration was evaluated using a PAMPA [47]. Ten commercial drugs, PBS solution at pH 7.4, DMSO and dodecane were purchased from Sigma, Acros organics, Merck, Aldrich and Fluka. The porcine polar brain lipid (PBL) (catalog no. 141101) was from Avanti Polar Lipids. The donor plate was a 96-well filtrate plate (Multiscreen® IP Sterile Plate PDVF membrane, pore size is 0.45 μM, catalog no. MAIPS4510) and the acceptor plate was an indented 96-well plate (Multiscreen®, catalog no. MAMCS9610) both from Millipore. Filter PDVF membrane units (diameter 30 mm, pore size 0.45 μm) from Symta were used to filter the samples. A 96-well plate UV reader (Thermoscientific, Multiskan spectrum) was used for the UV measurements. Test compounds [(3–5 mg of Caffeine, Enoxacine, Hydrocortisone, Desipramine, Ofloxacine, Piroxicam, Testosterone), (12 mg of Promazine) and 25 mg of Verapamile and Atenolol] were dissolved in DMSO (250 μL). 25 μl of this compound stock solution was taken and 225 μL of DMSO and 4750 μL of PBS pH = 7.4 buffer were added to reach 5% of DMSO concentration in the experiment. These solutions were filtered. The acceptor 96-well microplate was filled with 180 μL of PBS/DMSO (95/5). The donor 96-well plate was coated with 4 μL of porcine brain lipid in dodecane (20 mg/mL) and after 5 min, 180 μL of each compound solution was added. 1–2 mg of every compound to be determined their ability to pass the brain barrier were dissolved in 250 μL of DMSO and 4750 μL of PBS pH = 7.4 buffer, filtered and then added to the donor 96-well plate. Then the donor plate was carefully put on the acceptor plate to form a "sandwich", which was left for 1 h and 45 min in orbital shaking (rpm) at 25 °C. During this time the compounds diffused from the donor plate through the brain lipid membrane into the acceptor plate. After incubation, the donor plate was removed. UV plate reader determined the concentration of compounds and commercial drugs in the acceptor and the donor wells. Every sample was analyzed at three to five wavelengths, in 3 wells and in two independent runs. Results are given as the mean [standard deviation (SD)] and the average of the two runs is reported. 10 quality control compounds (previously mentioned) of known BBB permeability were included in each experiment to validate the analysis set.

CRediT authorship contribution statement

Sara Calenda: Writing – review & editing, Writing – original draft, Visualization, Validation, Methodology, Investigation, Formal analysis, Conceptualization. **Katarina Mihajlovic:** Writing – review & editing, Writing – original draft, Visualization, Validation, Methodology, Investigation, Formal analysis. **Flavia Varano:** Writing – review & editing, Formal analysis. **Daniela Catarzi:** Writing – review & editing, Formal analysis. **Costanza Ceni:** Writing – review & editing, Formal analysis. **Elisa Marinari:** Writing – review & editing, Formal analysis. **Giulia Vagnoni:** Writing – review & editing, Formal analysis. **Marta Menicatti:** Writing – original draft, Methodology, Investigation, Formal analysis, Data curation. **Gian Luca Bartolucci:** Writing – review & editing, Writing – original draft, Methodology, Data curation, Conceptualization. **Diego Dal Ben:** Writing – original draft, Visualization, Methodology, Investigation, Formal analysis. **Rosaria Volpini:** Writing – review & editing, Formal analysis. **Katia Varani:** Writing – review & editing, Data curation. **Chiara Contri:** Writing – original draft, Visualization, Investigation. **Fabrizio Vincenzi:** Writing – review & editing, Writing – original draft, Methodology, Formal analysis, Data curation. **Ana Martinez:** Writing – review & editing, Formal analysis, Data curation. **Loreto Martinez Gonzales:** Writing – original draft, Methodology, Investigation, Formal analysis. **Milorad Dragic:** Methodology, Investigation, Formal analysis, Conceptualization. **Miloš Mojović:** Writing – review & editing, Formal analysis, Conceptualization. **Đura Nakarada:** Writing – original draft, Methodology, Investigation. **Ivana Stevanovic:** Writing – review & editing, Formal analysis, Data curation. **Nadežda Nedeljkovic:** Writing – review & editing, Funding acquisition, Formal analysis, Data curation, Conceptualization. **Vittoria Colotta:**

Writing – review & editing, Writing – original draft, Supervision, Funding acquisition, Conceptualization.

Declaration of competing interest

The authors declare that they have no known competing financial interests or personal relationships that could have appeared to influence the work reported in this paper.

Acknowledgments

The work was funded by NEXT-GENERATION-EU-National Recovery and Resilience Plan (NRRP), Mission 4-Component 2. Inv.1.5-Ministry of University and Research (MUR), ECS_00000017 – MUR DD 1055, 23.06.2022, CUP B83C22003920001. Project title Tuscany Health Ecosystem, Spoke 8 (S.C.; D.C.; V.C.; F.V.); Ministry of Science, Technological Development and Innovation of the Republic of Serbia, grants Nos. 451-03-34/2026-03/200178 and 451-03-33/2026-03/200178 (N. N.).

Appendix A. Supplementary data

Supplementary data to this article can be found online at https://doi.org/10.1016/j.bioorg.2026.110166.

Data availability

No data was used for the research described in the article.

References

[1] W. Zhang, D. Xiao, Q. Mao, H. Xia, Role of neuroinflammation in neurodegeneration development, Sig. Transduct. Target. Ther. 8 (2023) 267, https://doi.org/10.1038/s41392-023-01486-5.
[2] J.M. Frischer, S. Bramow, A. Dal-Bianco, C.F. Lucchinetti, H. Rauschka, M. Schmidbauer, H. Laursen, P.S. Sorensen, H. Lassmann, The relation between inflammation and neurodegeneration in multiple sclerosis brains, Brain 132 (2009) 1175–1189, https://doi.org/10.1093/brain/awp070.
[3] T. Chitnis, H.L. Weiner, CNS inflammation and neurodegeneration, J. Clin. Invest. 127 (2017) 3577–3587, https://doi.org/10.1172/JCI90609.
[4] K.A. Jacobson, Introduction to adenosine receptors as therapeutic targets, Handb. Exp. Pharmacol. 193 (2009) 1–24, https://doi.org/10.1007/978-3-540-89615-9_1.
[5] B.B. Fredholm, A.P. Ijzerman, K.A. Jacobson, J. Linden, C.E. Müller, International Union of Basic and Clinical Pharmacology. LXXXI. Nomenclature and classification of adenosine receptors—an update, Pharmacol. Rev. 63 (2011) 1–34, https://doi.org/10.1124/PR.110.003285.
[6] S. Gessi, S. Merighi, K. Varani, P.A. Borea, Adenosine receptors in health and disease, Adv. Pharmacol. 61 (2011) 41–75, https://doi.org/10.1016/B978-0-12-385526-8.00002-3.
[7] P.A. Borea, K. Varani, F. Vincenzi, P.G. Baraldi, M.A. Tabrizi, S. Merighi, S. Gessi, The A3 adenosine receptor: history and perspectives, Pharmacol. Rev. 67 (2015) 74–102, https://doi.org/10.1124/PR.113.008540.
[8] V. Salmaso, S. Menin, S. Moro, G. Spalluto, S. Federico, Adenosine receptors in neuroinflammation and neurodegeneration, Cells 14 (2025) 1585, https://doi.org/10.3390/cells14201585.
[9] S. Pasquini, C. Contri, P.A. Borea, F. Vincenzi, K. Varani, Adenosine and inflammation: here, there and everywhere, Int. J. Mol. Sci. 22 (2021) 7685, https://doi.org/10.3390/ijms22147685.
[10] L. Zhong, Q. Peng, X. Zeng, The role of adenosine A1 receptor on immune cells, Inflamm. Res. 71 (2022) 1203–1212, https://doi.org/10.1007/S00011-022-01607-W.
[11] J. Stockwell, E. Jakova, F.S. Cayabyab, Adenosine A1 and A2A receptors in the brain: current research and their role in neurodegeneration, Molecules 22 (2017) 676, https://doi.org/10.3390/molecules22040676.
[12] Z.G. Gao, M. Haddad, K.A. Jacobson, A2B adenosine receptor signaling and regulation, Purinergic Signal 21 (2025) 201–220, https://doi.org/10.1007/S11302-024-10025-Y.
[13] J. Ingwersen, B. Wingerath, J. Graf, K. Lepka, M. Hofrichter, F. Schröter, F. Wedekind, A. Bauer, J. Schrader, H.-P. Hartung, T. Prozorovski, O. Aktas, Dual roles of the adenosine A2a receptor in autoimmune neuroinflammation, J. Neuroinflammation 13 (2016) 48, https://doi.org/10.1186/S12974-016-0512-Z.
[14] W. Wei, C. Du, J. Lv, G. Zhao, Z. Li, Z. Wu, G. Haskó, X. Xie, Blocking A2B adenosine receptor alleviates pathogenesis of experimental autoimmune encephalomyelitis via inhibition of IL-6 production and Th17 differentiation, J. Immunol. 190 (2013) 138–146, https://doi.org/10.4049/jimmunol.1103721.
[15] U.C. Dash, N.K. Bhol, S.K. Swain, R.R. Samal, P.K. Nayak, V. Raina, S.K. Panda, R. G. Kerry, A.K. Duttaroy, A.B. Jena, Oxidative stress and inflammation in the pathogenesis of neurological disorders: mechanisms and implications, Acta Pharm. Sin. B 15 (2025) 15–34, https://doi.org/10.1016/j.apsb.2024.10.004.
[16] T. Hussain, B. Tan, Y. Yin, F. Blachier, M.C.B. Tossou, N. Rahu, Oxidative stress and inflammation: what polyphenols can do for us? Oxid. Med. Cell. Longev. (2016) 7432797 https://doi.org/10.1155/2016/7432797.
[17] L.T. Zheng, G.M. Ryu, B.M. Kwon, W.H. Lee, K. Suk, Anti-inflammatory effects of catechols in lipopolysaccharide-stimulated microglia cells: inhibition of microglial neurotoxicity, Eur. J. Pharmacol. 588 (2008) 106–113, https://doi.org/10.1016/j.ejphar.2008.04.035.
[18] F. Superti, R. Russo, Alpha-lipoic acid: biological mechanisms and health benefits, Antioxidants 13 (2024) 1228, https://doi.org/10.3390/antiox13101228.
[19] H. Xie, X. Yang, Y. Cao, X. Long, H. Shang, Z. Jia, Role of lipoic acid in multiple sclerosis, CNS Neurosci. Ther. 28 (2021) 319, https://doi.org/10.1111/cns.13793.
[20] M. Falsini, D. Catarzi, F. Varano, C. Ceni, D. Dal Ben, G. Marucci, M. Buccioni, R. Volpini, L. Di Cesare Mannelli, E. Lucarini, C. Ghelardini, G. Bartolucci, M. Menicatti, V. Colotta, Antioxidant-conjugated 1,2,4-triazolo[4,3-a]pyrazin-3-one derivatives: highly potent and selective human A2A adenosine receptor antagonists possessing protective efficacy in neuropathic pain, J. Med. Chem. 62 (2019) 8511–8531, https://doi.org/10.1021/acs.jmedchem.9b00778.
[21] S. Calenda, C. Ceni, D. Catarzi, F. Varano, G. Vagnoni, G. Bartolucci, M. Menicatti, G. Marucci, M. Buccioni, D. Dal Ben, R. Volpini, A. Capperucci, D. Tanini, M. Venturini, E. Landucci, C. Santalmasi, F. Cherchi, C. Mazzantini, A.M. Pugliese, D.E. Pellegrini-Giampietro, V. Colotta, 8-Amino-1,2,4-triazolo[4,3-a]pyrazin-3-one derivatives hybridized with antioxidants: new highly potent and selective human A2A adenosine receptor antagonists as useful agents against cerebral ischemia, Bioorg. Chem. 164 (2025) 108855, https://doi.org/10.1016/j.bioorg.2025.108855.
[22] F. Varano, D. Catarzi, M. Falsini, D. Dal Ben, M. Buccioni, G. Marucci, R. Volpini, V. Colotta, Novel human adenosine receptor antagonists based on the 7-amino-thiazolo[5,4-d]pyrimidine scaffold. Structural investigations at the 2-, 5- and 7-positions to enhance affinity and tune selectivity, Bioorg. Med. Chem. Lett. 29 (2019) 563–569, https://doi.org/10.1016/j.bmcl.2018.12.062.
[23] F. Cherchi, L. Frulloni, M. Venturini, G. Magni, S. Calenda, R. Innocenti, F. Varano, D. Catarzi, C. Ceni, G. Vagnoni, V. Colotta, F. Vincenzi, K. Varani, M. Prisinzano, C. Donati, F. Cencetti, E. Coppi, A.M. Pugliese, Adenosine A2A receptor blockade promotes oligodendrocyte differentiation and myelination: highlighting the potency of an edaravone-conjugated A2A receptor antagonist, Neuropharmacology 282 (2026) 110724, https://doi.org/10.1016/j.neuropharm.2025.110724.
[24] F. Varano, D. Catarzi, F. Vincenzi, M. Betti, M. Falsini, A. Ravani, P.A. Borea, V. Colotta, K. Varani, Design, synthesis, and pharmacological characterization of 2-(2-furanyl)thiazolo[5,4-d]pyrimidine-5,7-diamine derivatives: new highly potent A2A adenosine receptor inverse agonists with antinociceptive activity, J. Med. Chem. 59 (2016) 10564–10576, https://doi.org/10.1021/acs.jmedchem.6b01068.
[25] J. Liu, "Modified proteins and protein binders," WO2022194087A1, 2022.
[26] M.L. Bolognesi, C. Bergamini, R. Fato, J. Oiry, J.J. Vasseur, M. Smietana, Synthesis of new lipoic acid conjugates and evaluation of their free radical scavenging and neuroprotective activities, Chem. Biol. Drug Des. 83 (2014) 688–696, https://doi.org/10.1111/cbdd.12282.
[27] T. Weinert, N. Olieric, R. Cheng, S. Brünle, D. James, D. Ozerov, D. Gashi, L. Vera, M. Marsh, K. Jaeger, F. Dworkowski, E. Panepucci, S. Basu, P. Skopintsev, A. S. Doré, T. Geng, R.M. Cooke, M. Liang, A.E. Prota, V. Panneels, P. Nogly, U. Ermler, G. Schertler, M. Hennig, M.O. Steinmetz, M. Wang, J. Standfuss, Serial millisecond crystallography for routine room-temperature structure determination at synchrotrons, Nat. Commun. 8 (2017) 542, https://doi.org/10.1038/s41467-017-00630-4.
[28] G. Jones, P. Willett, R.C. Glen, A.R. Leach, R. Taylor, Development and validation of a genetic algorithm for flexible docking, J. Mol. Biol. 267 (1997) 727–748, https://doi.org/10.1006/jmbi.1996.0897.
[29] L. Xu, D. He, Y. Bai, Microglia-mediated inflammation and neurodegenerative disease, Mol. Neurobiol. 53 (2016) 6709–6715, https://doi.org/10.1007/s12035-015-9593-4.
[30] D.S.A. Simpson, P.L. Oliver, ROS generation in microglia: understanding oxidative stress and inflammation in neurodegenerative disease, Antioxidants 9 (2020) 1–27, https://doi.org/10.3390/antiox9080743.
[31] P. Magni, M. Ruscica, E. Dozio, E. Rizzi, G. Beretta, R.M. Facino, Parthenolide inhibits the LPS-induced secretion of IL-6 and TNF-α and NF-κB nuclear translocation in BV-2 microglia, Phytother. Res. 26 (2012) 1405–1409, https://doi.org/10.1002/ptr.3732.
[32] S.K. Choi, Y.S. Park, D.K. Choi, H.I. Chang, Effects of astaxanthin on the production of NO and the expression of COX-2 and iNOS in LPS-stimulated BV2 microglial cells, J. Microbiol. Biotechnol. 18 (2008) 1990–1996, https://doi.org/10.4014/jmb.0800.489.
[33] K. Barber, P. Mendonca, J.A. Evans, K.F. Soliman, Antioxidant and anti-inflammatory mechanisms of cardamonin through Nrf2 activation and NF-kB suppression in LPS-activated BV-2 microglial cells, Int. J. Mol. Sci. 24 (2023) 10872, https://doi.org/10.3390/ijms241310872.
[34] F. Aktan, iNOS-mediated nitric oxide production and its regulation, Life Sci. 75 (2004) 639–653, https://doi.org/10.1016/j.lfs.2003.10.042.
[35] S. Merighi, P.A. Borea, S. Gessi, Adenosine receptors and diabetes: focus on the A2B adenosine receptor subtype, Pharmacol. Res. 99 (2015) 229–236, https://doi.org/10.1016/j.phrs.2015.06.015.
[36] Z. Xu, B.R. Wang, X. Wang, F. Kuang, X.L. Duan, X.Y. Jiao, G. Ju, ERK1/2 and p38 mitogen-activated protein kinase mediate iNOS-induced spinal neuron

degeneration after acute traumatic spinal cord injury, Life Sci. 79 (2006) 1895–1905, https://doi.org/10.1016/j.lfs.2006.06.023.
[37] J. Wang, D. Wang, X. Zheng, Y. Li, Y. Li, T. Ma, J. Li, J. Sun, Y. Wang, Q. Ma, A2B adenosine receptor inhibition ameliorates hypoxic-ischemic injury in neonatal mice via PKC/Erk/Creb/HIF-1α signaling pathway, Brain Res. 1782 (2022) 147837, https://doi.org/10.1016/j.brainres.2022.147837.
[38] M. Colella, M. Zinni, J. Pansiot, M. Cassanello, J. Mairesse, L. Ramenghi, O. Baud, Modulation of microglial activation by adenosine A2a receptor in animal models of perinatal brain injury, Front. Neurol. 9 (2018) 355877, https://doi.org/10.3389/fneur.2018.00605.
[39] S. Merighi, S. Bencivenni, F. Vincenzi, K. Varani, P.A. Borea, S. Gessi, A2B adenosine receptors stimulate IL-6 production in primary murine microglia through p38 MAPK kinase pathway, Pharmacol. Res. 117 (2017) 9–19, https://doi.org/10.1016/j.phrs.2016.11.024.
[40] S.M. Kim, J.S. Ha, A.R. Han, S.W. Cho, S.J. Yang, Effects of α-lipoic acid on LPS-induced neuroinflammation and NLRP3 inflammasome activation through the regulation of BV-2 microglial cells activation, BMB Rep. 52 (2019) 613–618, https://doi.org/10.5483/bmbrep.2019.52.10.026.
[41] C.S. Dzah, H. Zhang, V. Gobe, D. Asante-Donyinah, Y. Duan, Anti-and pro-oxidant properties of polyphenols and their role in modulating glutathione synthesis, activity and cellular redox potential: potential synergies for disease management, Adv. Redox Res. 11 (2024) 100099, https://doi.org/10.1016/j.arres.2024.100099.
[42] C.M.C. Andrés, J.M. Pérez de la Lastra, C.A. Juan, F.J. Plou, E. Pérez-Lebeña, Polyphenols as antioxidant/pro-oxidant compounds and donors of reducing species: relationship with human antioxidant metabolism, Processes 11 (2023) 2771, https://doi.org/10.3390/pr11092771.
[43] A. Kumar, S.H. Chen, M.B. Kadiiska, J.S. Hong, J. Zielonka, B. Kalyanaraman, R. P. Mason, Inducible nitric oxide synthase is key to peroxynitrite-mediated, LPS-induced protein radical formation in murine microglial BV2 cells, Free Radic. Biol. Med. 73 (2014) 51–59, https://doi.org/10.1016/j.freeradbiomed.2014.04.014.
[44] F.A. Villamena, J.L. Zweier, Detection of reactive oxygen and nitrogen species by EPR spin trapping, Antiox. Redox. Signal 6 (2004) 619–629, https://doi.org/10.1089/152308604773934387.
[45] F.L. Cardoso, D. Brites, M.A. Brito, Looking at the blood–brain barrier: molecular anatomy and possible investigation approaches, Brain Res. Rev. 64 (2010) 328–363, https://doi.org/10.1016/j.brainresrev.2010.05.003.
[46] J. Van Asperen, U. Mayer, O. Van Tellingen, J.H. Beijnen, The functional role of P-glycoprotein in the blood–brain barrier, J. Pharm. Sci. 86 (1997) 881–884, https://doi.org/10.1021/js9701364.
[47] L. Di, E.H. Kerns, K. Fan, O.J. McConnell, G.T. Carter, High throughput artificial membrane permeability assay for blood–brain barrier, Eur. J. Med. Chem. 38 (2003) 223–232, https://doi.org/10.1016/S0223-5234(03)00012-6.
[48] P. Crivori, G. Cruciani, P.-A. Carrupt, B. Testa, Predicting blood-brain barrier permeation from three-dimensional molecular structure, J. Med. Chem. 43 (2000) 2204–2216, https://doi.org/10.1021/JM990968.
[49] F. Vincenzi, M. Targa, R. Romagnoli, S. Merighi, S. Gessi, P.G. Baraldi, P.A. Borea, K. Varani, TRR469, a potent A1 adenosine receptor allosteric modulator, exhibits anti-nociceptive properties in acute and neuropathic pain models in mice, Neuropharmacology 81 (2014) 6–14, https://doi.org/10.1016/j.neuropharm.2014.01.028.
[50] K. Varani, A. Massara, F. Vincenzi, A. Tosi, M. Padovan, F. Trotta, P.A. Borea, Normalization of A2A and A3 adenosine receptor up-regulation in rheumatoid arthritis patients by treatment with anti–tumor necrosis factor α but not methotrexate, Arthritis Rheum. 60 (2009) 2880–2891, https://doi.org/10.1002/art.24794.
[51] K. Varani, S. Merighi, S. Gessi, K.N. Klotz, E. Leung, P.G. Baraldi, B. Cacciari, R. Romagnoli, G. Spalluto, P.A. Borea, [3H]MRE 3008F20: a novel antagonist radioligand for the pharmacological and biochemical characterization of human A3 adenosine receptors, Mol. Pharmacol. 57 (2000) 968–975, https://doi.org/10.1016/S0026-895X(24)26507-X.
[52] A. Ravani, F. Vincenzi, A. Bortoluzzi, M. Padovan, S. Pasquini, S. Gessi, S. Merighi, P.A. Borea, M. Govoni, K. Varani, Role and function of A2A and A3 adenosine receptors in patients with ankylosing spondylitis, psoriatic arthritis and rheumatoid arthritis, Int. J. Mol. Sci. 18 (2017) 697, https://doi.org/10.3390/ijms18040697.
[53] H.Y. Nam, J.H. Nam, G. Yoon, J.Y. Lee, Y. Nam, H.J. Kang, H.J. Cho, J. Kim, H. S. Hoe, Ibrutinib suppresses LPS-induced neuroinflammatory responses in BV2 microglial cells and wild-type mice, J. Neuroinflammation 15 (2018) 271, https://doi.org/10.1186/S12974-018-1308-0.
[54] S.T. Nguyen, H.T.L. Nguyen, K.D. Truong, Comparative cytotoxic effects of methanol, ethanol and DMSO on human cancer cell lines, Biomed. Res. Ther. 7 (2020) 3855–3859, https://doi.org/10.15419/bmrat.v7I7.614.
[55] A. Villacara, K. Kumami, T. Yamamoto, B.B. Ulja, M. Spatz, Ischemic modification of cerebrocortical membranes: 5-hydroxytryptamine receptors, fluidity, and inducible in vitro lipid peroxidation, J. Neurochem. 53 (1989) 595–601, https://doi.org/10.1111/J.1471-4159.1989.TB07375.X.
[56] C. Auclair, E. Voisin, Nitroblue tetrazolium reduction, in: Hdbk Methods for Oxygen Radical Research, 3rd ed., CRC Press, Florida, 1985, pp. 123–132.
[57] S.J. Stohs, T.A. Lawson, L. Anderson, E. Bueding, Effects of oltipraz, BHA, ADT and cabbage on glutathione metabolism, DNA damage and lipid peroxidation in old mice, Mech. Ageing Dev. 37 (1986) 137–145, https://doi.org/10.1016/0047-6374(86)90071-0.
[58] M. Sun, S. Zigman, An improved spectrophotometric assay for superoxide dismutase based on epinephrine autoxidation, Anal. Biochem. 90 (1978) 81–89, https://doi.org/10.1016/0003-2697(78)90010-6.
[59] L. Góth, A simple method for determination of serum catalase activity and revision of reference range, Clin. Chim. Acta 196 (1991) 143–151, https://doi.org/10.1016/0009-8981(91)90067-M.
[60] R.C.C. Chang, C. Rota, R.E. Glover, R.P. Mason, J.S. Hong, A novel effect of an opioid receptor antagonist, naloxone, on the production of reactive oxygen species by microglia: a study by electron paramagnetic resonance spectroscopy, Brain Res. 854 (2000) 224–229, https://doi.org/10.1016/S0006-8993(99)02267-2.
[61] M. Mojović, M. Vuletić, G.G. Bačić, Detection of oxygen-centered radicals using EPR spin-trap DEPMPO: the effect of oxygen, Ann. N. Y. Acad. Sci. 1048 (2005) 471–475, https://doi.org/10.1196/annals.1342.069.